AGU PUBLICATIONS

JGR

Journal of Geophysical Research: Atmospheres

RESEARCH ARTICLE
10.1002/2013JD020992

Key Points:
- Measurements of HCl in the polluted MBL with novel instrumentation
- Investigations of Cl atom production rates from HCl
- Investigation of gas- to particulate-phase partitioning

Correspondence to:
T. H. Bertram,
thbertram@ucsd.edu

Citation:
Crisp, T. A., B. M. Lerner, E. J. Williams, P. K. Quinn, T. S. Bates, and T. H. Bertram (2014), Observations of gas phase hydrochloric acid in the polluted marine boundary layer, *J. Geophys. Res. Atmos.*, *119*, 6897–6915, doi:10.1002/2013JD020992.

Received 7 OCT 2013
Accepted 1 MAY 2014
Accepted article online 6 MAY 2014
Published online 10 JUN 2014

Observations of gas phase hydrochloric acid in the polluted marine boundary layer

Timia A. Crisp[1], Brian M. Lerner[2,3], Eric J. Williams[2,3], Patricia K. Quinn[4], Timothy S. Bates[4], and Timothy H. Bertram[1]

[1]Department of Chemistry and Biochemistry, University of California, San Diego, La Jolla, California, USA, [2]Chemical Sciences Division, Earth System Research Laboratory, NOAA, Boulder, Colorado, USA, [3]Cooperative Institute for Research in Environmental Sciences, University of Colorado Boulder, Boulder, Colorado, USA, [4]Pacific Marine Environmental Laboratory, NOAA, Seattle, Washington, USA

Abstract Ship-based measurements of gas phase hydrochloric acid (HCl), particulate chloride (pCl^-), and reactive nitrogen oxides (NO_y) were made in the polluted marine boundary layer along the California coastline during spring 2010. These observations are used to assess both the rate of Cl atom production from HCl and the role of direct HCl emissions and subsequent partitioning as a source for pCl^-. Observations of HCl made in coastal Southern California are broadly correlated with NO_z ($NO_z \equiv NO_y - NO_x$), peaking at 11 A.M. The observed median HCl mixing ratio in Southern California is 1.3 ppb (interquartile range: 0.53–2.7 ppb), as compared to 0.19 ppb (interquartile range: 0.10–0.38 ppb) measured along the Sacramento River between San Francisco and Sacramento. Concurrent measurements of aerosol ion chemistry indicate that aerosol particles sampled in Northern California are heavily depleted in Cl^-, corresponding to a mean pCl^- deficit of 0.05 ± 0.03 (1σ) ppb for sub-10 μm aerosol particles. In comparison, aerosols measured in Southern California indicate that over 25% of particles showed an addition of Cl^- to the particle population. Observations presented here suggest that primary sources of HCl, or gas phase chlorine precursors to HCl, are likely underestimated in the California Air Resource Board emissions inventory. These results highlight the need for future field observations designed to better constrain direct reactive halogen emissions.

1. Introduction

Chlorine atoms (Cl) may play an important role in controlling the lifetime of methane [*Finlayson-Pitts*, 1993; *Pszenny et al.*, 2007; *Singh and Kasting*, 1988; *von Glasow and Crutzen*, 2003], impact net ozone (O_3) production rates in the marine boundary layer [*Martinez et al.*, 1999; *Pszenny et al.*, 2004; *Riedel et al.*, 2012; *Riedel et al.*, 2013], and initialize VOC oxidation and peroxy radical (RO_2) production [*Finlayson-Pitts*, 1993; *Knipping and Dabdub*, 2002; *Pszenny et al.*, 1993; *Riedel et al.*, 2012; *Riedel et al.*, 2013; *Saiz-Lopez and von Glasow*, 2012; *Young et al.*, 2014]. However, to date, no direct observations of Cl atom concentrations have been reported in either the remote marine boundary layer or in polluted coastal regions. As a result, current estimates of Cl atom concentrations are inferred through steady state approximation [*Finlayson-Pitts*, 1993], observations of the net impact of Cl atoms on methane isotopologues [*Allan et al.*, 2005; *Platt et al.*, 2004], and through observations of the relative concentrations of nonmethane hydrocarbons [*Rudolph et al.*, 1997; *Singh et al.*, 1996; *Wingenter et al.*, 1999, 1996, 2005]. In order to accurately assess the impact of Cl atom chemistry on the oxidative capacity of the troposphere using steady state approaches, a complete description of Cl atom precursors, Cl atom loss mechanisms, and the reaction kinetics that determine both Cl atom production and loss rates are required.

Cl atoms are primarily generated in the marine boundary layer from the oxidation of HCl by hydroxyl radicals (OH) and the photolysis of photolabile chlorine reservoir compounds (e.g., $ClNO_2$, Cl_2, and BrCl) that are either directly emitted to the atmosphere or formed through heterogeneous and multiphase reactions on chloride-containing aerosols [*Finlayson-Pitts*, 1993; *Graedel and Keene*, 1995; *Riedel et al.*, 2012; *Singh and Kasting*, 1988; *von Glasow and Crutzen*, 2003; *Wingenter et al.*, 1996]. Under high-NO_x conditions characteristic of the polluted marine boundary layer, chlorine activation from sea spray aerosol is primarily initiated by the reactive uptake of nitric acid (HNO_3) and dinitrogen pentoxide (N_2O_5) [*Finlayson-Pitts*, 1993; *Finlayson-Pitts*, 2009; *Osthoff et al.*, 2008], resulting in the production of Cl atom precursors HCl, $ClNO_2$, and Cl_2 [*Saiz-Lopez and von Glasow*, 2012; *von Glasow and Crutzen*, 2003]. HCl is formed in situ through the partitioning of strong

mineral acids, such as HNO_3 and H_2SO_4, as well as low volatility organic acids onto chloride-containing aerosol (e.g., (R1)) [*Erickson et al*., 1999; *Gard et al*., 1998; *Keene et al*., 1999; *Laskin et al*., 2012], and through hydrogen abstraction by Cl atom reactions with volatile organic compounds (R2) [*Graedel and Keene*, 1995]. However, the chemistry that governs chlorine activation from sea spray aerosol under low-NO_x conditions is less well understood. Recent work by *Laskin et al*. [2012] suggests that acid displacement processes involving low-volatility organic acids may play an important role in HCl volatilization from particles. In addition to the oxidation of HCl, laboratory measurements and field observations suggest that autocatalytic multiphase reactions involving HOCl may play an important role in sustaining elevated Cl atom concentrations in the remote marine boundary layer [*Lawler et al*., 2011; *Pechtl and von Glasow*, 2007; *Vogt et al*., 1996].

$$HNO_3(g) + Cl^-(aq) \rightarrow HCl(g) + NO_3^-(aq) \quad \text{(R1)}$$

$$RH(g) + Cl\cdot(g) \rightarrow R\cdot(g) + HCl(g) \quad \text{(R2)}$$

There has been renewed interest in the coupling of reactive nitrogen oxides and chlorine cycles following recent observations of elevated mixing ratios of $ClNO_2$ in both coastal [*Osthoff et al*., 2008] and continental regions [*Thornton et al*., 2010]. These observations have led to a reassessment of the reactive chlorine budget on regional and global scales, suggesting a crucial role for HCl gas-particle partitioning in sustaining aerosol chloride concentrations [*Brown and Stutz*, 2012; *Osthoff et al*., 2008; *Riedel et al*., 2012; *Sarwar et al*., 2012; *Thornton et al*., 2010]. Observations of elevated $ClNO_2$ (as high as 600 pptv) in continental air masses [*Thornton et al*., 2010], which are traditionally thought to have limited Cl-containing aerosol, suggest that direct HCl emission from anthropogenic activities (e.g., biomass burning, combustion, and industrial processes) may contribute significantly to the chloride content of continental particles.

Gas phase HCl is directly emitted to the atmosphere from the combustion of chloride-containing fuels (e.g., waste incineration, biomass burning, and coal combustion), volcanic emissions, water treatment, and emissions during manufacturing processes [*Keene et al*., 1999; *Khalil et al*., 1999; *McCulloch et al*., 1999]. *Graedel and Keene* [1995] estimated the globally integrated annual flux of HCl via sea-salt dechlorination to be 50 Tg Cl yr^{-1} by assuming that the primary sea-salt dechlorination pathway is acid displacement, an average HCl mixing ratio of 200 pptv, and a deposition lifetime (τ_{dep}) for HCl of 1–2 days. However, *Erickson et al*. [1999] could account for only 7.6 Tg Cl yr^{-1} from the uptake of strong acids such as H_2SO_4 and HNO_3 on chloride-containing particles. This lower estimate may be due to an underestimation of the incorporation of H_2SO_4 into sea-salt aerosol and hence HCl volatilization or missing atmospheric processes that result in sea-salt dechlorination. Recently, it has been suggested that organic acids may contribute to HCl volatilization from sea-salt particles, potentially accounting for some of the discrepancy [*Laskin et al*., 2012]. Direct emission of HCl has been estimated to be < 6.3 Tg Cl yr^{-1}, 4.6 Tg Cl yr^{-1}, and 2 Tg Cl yr^{-1} for biomass burning [*Lobert et al*., 1999], coal combustion, and waste incineration [*McCulloch et al*., 1999], respectively, based upon available inventories, including J. A. Logan and R. Yevich (unpublished manuscripts, 1998) and the *Agency*, *O. I. E*. [1992]. However, the relative strengths of direct HCl emission and secondary HCl production are highly variable spatially, where sea-salt dechlorination is thought to dominate in the marine boundary layer, while continental regions are likely to be more directly influenced by biomass burning, coal combustion, and waste incineration processes.

Figures 1b and 1c show the total anthropogenic HCl primary emissions and HCl production rate from sea-salt dechlorination, respectively, as determined by the Reactive Chlorine Emissions Inventory (RCEI) as part of the Global Emission Inventory Activity (GEIA) initiative [*Keene et al*., 1999]. Sea-salt dechlorination was estimated using the output of general circulation models, where the sea-salt distribution is a function of model surface wind stress, turbulence, and dry and wet deposition. HCl emissions were estimated [*Keene et al*., 1999; *Lobert et al*., 1999; *McCulloch et al*., 1999] using ambient measurements, population estimates, and current understanding of the reaction processes and rates. *Keene et al*. [1999] determined that combined coal combustion, incineration, and biomass burning yields 12.9 Tg Cl yr^{-1}, accounting for about 20% of the globally, annually averaged source of HCl in the troposphere. Based on the RCEI, anthropogenic sources are responsible for 2.59×10^{-2} Tg Cl yr^{-1} and 1.70×10^{-2} Tg Cl yr^{-1} for the Southern California (SC) and Northern California (NC) regions defined in Figure 1a, respectively, which accounts for 92% and 79% of the total HCl production in those regions, respectively. Sea-salt dechlorination therefore accounts for 8% and 21% of the total HCl RCEI emissions observed in the SC and NC regions, respectively.

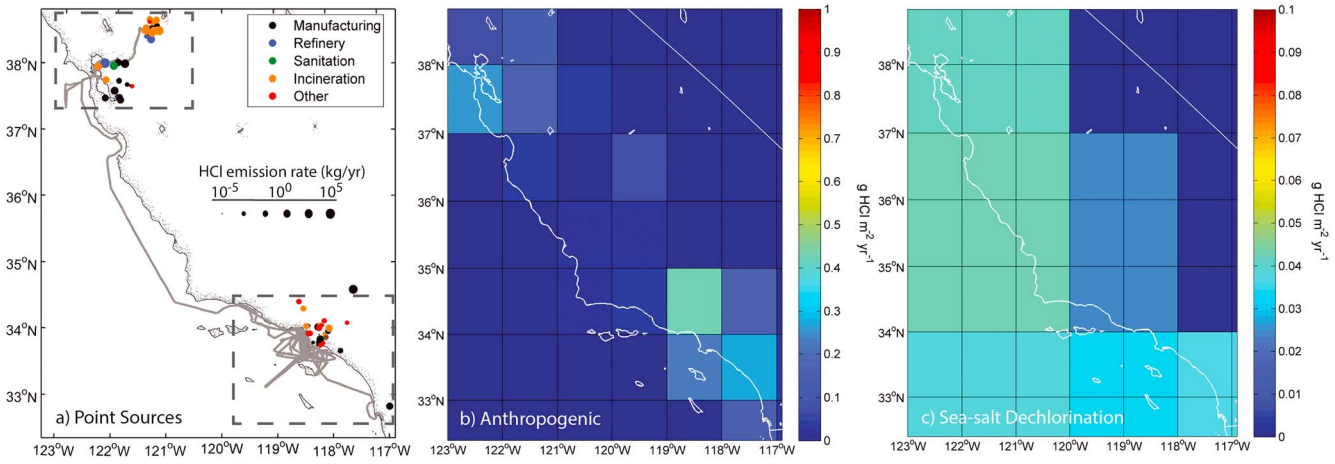

Figure 1. (a) The R/V *Atlantis* ship track during CalNex 2010. Colored circles depict primary HCl sources in Northern and Southern California as defined by the California Emissions Inventory Development and Reporting System (CEIDARS Database). The color and size of the circle represents the source type and HCl emission rate, respectively. The gray dashed boxes highlight Northern and Southern California sampling regions. (b) HCl emission rates from anthropogenic sources [*McCulloch et al.*, 1999] and (c) HCl production rates from sea-salt dechlorination reactions, as determined by the GEIA RCEI inventory [*Erickson et al.*, 1999; *Keene et al.*, 1999].

During California Research at the Nexus of Air Quality and Climate Change (CalNex) 2010, numerous known HCl anthropogenic sources were sampled, including ship emissions, oil refineries, waste incineration, sanitation, and manufacturing facilities. The location and emission rates (kg yr^{-1}), as determined using the California Emissions Inventory Development and Reporting System (CEIDARS Database) maintained by the California Environmental Protection Agency Air Resource Board (ARB), for all known HCl point sources in NC and SC California are shown in Figure 1a (V. Agusiegbe, personal communication, 2012) and are categorized by emission type: manufacturing, refinery, sanitation processes, incineration processes, and other emission sources. The emission type is represented by color, and the source strength is scaled to the size of the symbol. HCl emissions in the Northern and Southern California sampling domain collectively represent 1.22×10^{-4} Tg Cl yr^{-1} (38 sources) and 1.37×10^{-5} Tg Cl yr^{-1} (33 sources), respectively, significantly lower than the quoted anthropogenic source in the RCEI (1.70×10^{-2} Tg Cl yr^{-1} and 2.59×10^{-2} Tg Cl yr^{-1} for NC and SC, respectively). The discrepancy between the RCEI and the ARB inventory highlights (1) decreases in HCl emissions within the last decade, (2) spatial differences due to selection of sampling region, (3) inclusion of nonpoint sources other than sea-salt dechlorination (e.g., combustion in residential areas) that are not included in the ARB inventory, and/or more likely (4) the uncertainty in current HCl emissions from anthropogenic activities in both inventories. The RCEI HCl production rate from sea-salt dechlorination is estimated to be 4.54×10^{-3} and 2.30×10^{-3} Tg Cl yr^{-1} for NC and SC, respectively. If we assume HCl anthropogenic emissions from the ARB inventory and dechlorination rates from RCEI are correct, anthropogenic emissions would account for 2.6% and 0.6% of the total HCl production in NC and SC, respectively. This comparison illustrates sea-salt dechlorination is the major production pathway of HCl globally, as previous studies have reported [*Erickson et al.*, 1999; *Keene et al.*, 2007], though primary sources of HCl may be a significant local source of HCl.

The atmospheric lifetime of HCl is primarily controlled by wet and dry deposition, where the dry deposition velocity in marine environments has been estimated to range between 1 and 5 cm s^{-1} [*Finlayson-Pitts and Pitts*, 1999]. At a deposition rate of 1 cm s^{-1} and boundary layer height of 1 km, the lifetime of HCl with respect to dry deposition is 1.2 days. In comparison, the 24 h averaged lifetime of HCl with respect to OH oxidation is about 15 days (k_{OH+HCl} (298 K) = 8×10^{-13} cm^3 $molecule^{-1}$ s^{-1} and $[OH]_{24\ h} = 1 \times 10^6$ molecules cm^{-3}). Equilibrium partitioning of HCl to aerosols is pH dependent, where basic to circumneutral aerosols are expected to be a net sink for HCl [*Keene et al.*, 1990; *Watson et al.*, 1990]. Collectively, HCl lifetime in the marine boundary layer and thus the integrated Cl atom production rate stemming from HCl reactions with OH is a strong function of the deposition rate of HCl.

Accurate measurements of gas phase HCl are required to assess the production rate of Cl atoms via direct OH oxidation of HCl and to determine how HCl gas particle partitioning impacts particulate chloride concentrations

and subsequent activation of pCl^- to $ClNO_2$ via N_2O_5 heterogeneous reactions. In what follows, we first review previous HCl measurements in the polluted marine boundary layer and Cl atom production rates from HCl. We then describe a new set of high time resolution observations of HCl that are used to assess HCl sources to the polluted marine boundary layer and the direct production of Cl atoms from HCl oxidation.

1.1. Previous Tropospheric Measurements of HCl

Previous measurements of HCl mixing ratios in continental and marine air masses are summarized in Table 1. HCl mixing ratios are highest in polluted coastal regions and typically less than 1 ppbv over continental regions. In general, HCl is broadly correlated with HNO_3. The correlation is a result of the similar, fast deposition rate (1–5 cm s^{-1}) for HCl and HNO_3 [*Finlayson-Pitts and Pitts*, 1999; *Graedel and Keene*, 1995] as well as a common dependence of HNO_3 and HCl gas phase mixing ratios on solution acidity in phase partitioning and meteorological conditions (i.e., boundary layer height and relative humidity) [*Finlayson-Pitts and Pitts*, 1999]. HCl mixing ratios have been shown to exceed HNO_3 in polluted environments [*Johnson et al*., 1987; *Matsumoto and Okita*, 1998].

1.2. Chlorine Atom Production Rates From HCl

In polluted coastal regions, Cl atoms are produced from an array of reactive and photolabile chlorine-containing reservoirs (e.g., HCl, $ClNO_2$, Cl_2, and HOCl). Recently, *Riedel et al*. [2012] calculated Cl atom production rates from HCl, $ClNO_2$, and Cl_2 using observations made during the CalNex 2010 campaign in Southern California. The study indicated that diel averaged Cl atom production peaked at 6.4×10^5 molecule cm^{-3} s^{-1}, with 45%, 45%, and 10% of the production attributed to HCl, $ClNO_2$, and Cl_2, respectively [*Riedel et al*., 2012]. *Riedel et al*. [2012] compared the calculated Cl atom concentrations with modeled OH radical concentrations and suggested that Cl atoms may account for as much as 25% of the daily alkane oxidation, acting as a significant source of peroxy radicals. Recent model calculations in the Los Angeles region during CalNex suggest that the ratios of select VOCs may not be a sensitive indicator of the net impact of Cl atom chemistry, due to secondary production of OH following Cl oxidation of VOCs [*Young et al*., 2014].

In this study we describe direct, in situ measurements of HCl made using a newly developed chemical ionization time-of-flight mass spectrometer (CI-TOFMS) [*Bertram et al*., 2011] deployed aboard the R/V *Atlantis* during CalNex 2010. We use these observations, with coincident measurements of Cl-containing aerosol and gas phase reactive nitrogen oxides (NO_y), to assess the sources of HCl in the polluted marine boundary layer. In situ observations are combined with model calculations to provide constraints on the production rate of Cl atoms from HCl in polluted coastal regions of varying marine influence.

2. Experimental Methods

2.1. CalNex 2010 Campaign

The measurements discussed here were made aboard the R/V *Atlantis* as part of the CalNex 2010 multiplatform field campaign [*Ryerson et al*., 2013]. The R/V *Atlantis* provided a platform to measure the outflow of pollution in the marine boundary layer along the coast of California during May and June 2010. The R/V *Atlantis* ship track is shown in Figure 1a, where measurements have been divided into two sampling regions: Southern California (SC) and Northern California (NC). The SC region is defined as the coastal sampling area near Los Angeles between 121° and 117° W and 32° and 34.5° N. Conversely, the NC region comprises of the region between 37.5° and 39°N and 123° and 120°W, containing an inland region up to 160 km from the coast. HCl point sources in SC and NC regions, as defined by the CEIDARS Database (V. Agusiegbe, personal communication, 2012) are included in Figure 1a and are discussed further in section 3.6.

2.2. HCl Measurements via Chemical Ionization Mass Spectrometry

Chemical ionization time-of-flight mass spectrometry (CI-TOFMS) was used for the selective, sensitive detection of HCl. The instrument has been previously described by *Bertram et al*. [2011] with respect to the detection of gas phase formic acid. Here we describe the same instrument and ion chemistry as applied to the detection of HCl. Briefly, ambient air is pulled through a 7.6 m, 0.64 cm ID perfluoroalkoxy-heated inlet (temperature controlled to 35°C) at 10 standard liters per minute (sLpm) and 933 mbar, resulting in an average residence time of 1.5 s. The sample line was configured to subsample from the primary inlet flow at

Table 1. Previous Tropospheric HCl and Simultaneous HNO_3 Measurements

Location	Time	HCl Concentration Range[a] (pptv)	HNO_3 Concentration Range[a] (pptv)	Measurement Technique[b]	Reference
		Continental [c]			
Italy		100–2500			*Allegrini et al.* [1984]
Cabauw, Netherlands (51.55°N, 4.55°E)	Various seasons	60–2000	0–9000	Denuder/IC	*Erisman et al.* [1988]
Canada, Arizona, Kansas, Bermuda	Jun–Oct 1974	60–400		Filter/Neutron Activation	*RAHN et al.* [1976]
Manhattan, NY	Jul–Aug 1976	1000–9000(4000)			*Rahn et al.* [1979]
Reims, France (49°N, 4°E)	Dec 1978 to Jun 1979	1–100		IR Spectroscopy	*Marche et al.* [1980]
Columbus, Ohio	Sep 1980–Oct 1980	30–1000(350)	100–3000	Filter/IC	*Spicer* [1986]
Germany (50°N)		20–500			*Neissner* [1981]
multisite, Germany (50°N)	Mar–Apr 1981, Apr 1982	200–2000		Derivatization/GC	*Matusca et al.* [1984]
Paris, France	1983–1984	0–5000		Denuder/Titration	*Gounon and Milhau* [1986]
Leatherhead, England	May–Jun 1985	90–3800		Denuder/Ion-selective Electrode	*Dimmock and Marshall* [1987]
Japan (36°N)		30–100			*Iwasaki et al.* [1985]
Claremont, CA	Sep 1985	0–2000		Denuder/IC	*Appel et al.* [1991]
Claremont, CA	Sep 1985	0–1600		Dichotomous sampler	*John et al.* [1988]
Duebendorf, Switzerland	Oct 1985 to Feb 1986	50–2000(300)	50–900(200)	Denuder/IC	*Johnson et al.* [1987]
Glendora, CA	Aug 1986	0–850(500)	0–1100(400)	Filter/LC	*Grosjean* [1990]
multisite, LA/Riverside region	1986	400–1300[c]	100–2600[d]	Denuder/IC	*Eldering et al.* [1991]
multisite, SE England	Mar–Apr 1987	100–1200	200–700	Filter/IC	*Sturges and Harrison* [1989]
SE England	Feb 1987 to Jan 1988	200–1200(500)	60–1000(300)	Filter/IC	*Harrison and Allen* [1990]
Petten, Netherlands	Mar–Aug 1987	70–3000	40–6700	Denuder/IC	*Keuken et al.* [1988]
Arizona (33°)		200–1200			G. A. Dawson et al. (Tropospheric inorganic chlorine: Some concentration and isotope ratios, unpublished manuscript, 1989)
Sweden	Jan 1990	200–1000		Diffusion Scrubber/IC	*Lindgren* [1992]
Sweden	Jul 1990	100–600		Diffusion Scrubber/IC	*Lindgren* [1992]
Sweden	Sep 1990	20–300		Diffusion Scrubber/IC	*Lindgren* [1992]
Wolkersdorf, Austria (16°3′E, 48°2′N)	Nov 1990 to Oct 1991		100–1000	Denuder/IC	*Puxbaum et al.* [1985]
multisite, Metropolitan Tokyo area	Nov–Dec 1991	2100, max		Filter/IC	*Kaneyasu et al.* [1999]
UV Charlottesville, Virginia	Nov 1993	<40–2800		Tandem Mist Chamber/IC	*Maben et al.* [1995]
Nara, Japan (34.41°N, 135.48°E)	Jun 1994 to May 1995	800–1500 (1100)	30–4000(600)	Denuder/IC	*Matsumoto and Okita* [1998]
Manhattan, NY	Jul 1999 to Jun 2000	10–2000 (300)	20–5700(600)	Denuder/IC	*Bari et al.* [2003]
Bronx, NY	Jul 1999 to Jun 2000	10–1800 (300)	10–2800(400)	Denuder/IC	*Bari et al.* [2003]
Africa (Namibia, S. Africa, Malawi, Zambia)	Aug–Oct 2000			Tandem Mist Chamber/IC	*Keene et al.* [2006]
Sydney, FL (27.95°N, 82.23°W)	May 2002	<10–5600 (700)	10–3000(300)	Denuder/IC	*Dasgupta et al.* [2007]
Sacramento Delta, CA	May–Jun 2010	0–1900 (270)	210 to $> 1.5 \times 10^4$ (3300)[e]	Acetate CI-TOFMS	This study
Erie, CO (40.05°N, 105.01°W)	Feb–Mar 2011	23–1250	45 to > 1500	Tandem Mist Chamber/IC	*Young et al.* [2013]
		Marine[e]			
West African Coast	May–Jun 1977			Filter, Neutron Activation	*Kritz and Rancher* [1980]
Bermuda	Jul–Sep, 1988	200–400		Filter/IC	*Keene et al.* [1990]
U.S. East Coast	Jul–Sep, 1988	500–1200		Filter/IC	*Keene et al.* [1990]
Atlantic Ocean (28°N, 30°W)	24 Sep 1988	250, max	100	TDLAS	*Harris et al.* [1992]
Virginia Key, Miami, FL	Jan 1992	40–270	<25–40	Tandem Mist Chamber/IC	*Pszenny et al.* [1993]
Oki Island Monitoring Station, Japan	Feb–Mar 1994	>800, max		Diffusion Scrubber/IC	*Kajii et al.* [1997]
Tudor Hill, Bermuda (32°N, 64°W)	Apr–May 1996	100–900	40–500	Tandem Mist Chamber/IC	*Keene and Savoie* [1998]
Bellows Air Force Station, Oahu, Hawai'i (21°22′N, 157°42.8′W)	Sep 1999	30–300		Tandem Mist Chamber/IC	*Pszenny et al.* [2004]

AGU Journal of Geophysical Research: Atmospheres 10.1002/2013JD020992

Table 1. (continued)

Location	Time	HCl Concentration Range[a] (pptv)	HNO_3 Concentration Range[a] (pptv)	Measurement Technique[b]	Reference
Dumont d'Urville, Antarctica	Dec 2000 to Dec 2001	30–300	0–40	Tandem Mist Chamber/IC	*Jourdain and Legrand* [2002]
S. Carolina to Canada	Jul–Aug 2002	<25–4500	<25–6500	Tandem Mist Chamber/IC	*Keene et al.* [2004]
Germany to S. Africa	Oct–Nov 2003	20–1400	5–500	Tandem Mist Chamber/IC	*Keene et al.* [2009]
Appledore Island near ME (42.90°N, 70.62°W)	Jul–Aug 2004	5–5800(600)	0–8000	Tandem Mist Chamber/IC	*Keene et al.* [2007]
N. Pacific Ocean near Alaska	May 2006	6–100(30)		SF_6 CIMS	*Kim et al.* [2008]
Sao Vicente Island, Cape Verde	May–Jun 2007	50–600	10–100	Tandem Mist Chamber/IC	*Lawler et al.* [2009]
Central California Coast	May–Jun 2010	0–2800(440)	40–620(120)[d]	Acetate CI-TOFMS	This study
Southern California Coast	May–Jun 2010	0 to > 16000(2200)	50 to > 4.0×10^4 (4500)[e]	Acetate CI-TOFMS	This study

[a]Mean values are shown in parentheses.
[b]Technique used to measure HCl.
[c]> 1 km from the coastline.
[d]Monthly averages; includes urban sites.
[e]NO_X concentration range.
[f]< 1 km from the coastline.

180° relative to the initial flow direction. As such, the reverse facing sample line acted to inertially remove large particles from the sampling line. Calculations based on particle stopping distance, constrained by the inlet flow rates and tube dimensions, suggest that the inlet served to remove particles larger than approximately 2.5 μm (d_p). Ambient air was subsampled again from the primary sample line through a critical orifice that restricted the flow entering the ion-molecule reaction region (IMR) to 1.7 sLpm, with the remaining flow pulled through a bypass line. In the IMR, HCl reacts with acetate ions (R3), which are produced by mixing 10 cm^3 min^{-1} STP of a saturated flow of acetic anhydride with 2200 cm^3 min^{-1} STP of ultrahigh purity (UHP) nitrogen (N_2) and passing the mixture over a ^{210}Po ionization source orthogonal to the IMR. Acetate ions react with HCl via proton abstraction, resulting in the formation of a chloride ion (R3) [*Veres et al.*, 2008].

$$CH_3C(O)O^- + HCl \rightarrow CH_3C(O)OH + Cl^- \quad \text{(R3)}$$

It is also possible for an acetate-HCl cluster to form in the IMR region. During CalNex, the CI-TOFMS was operating in a declustering configuration, where clusters were collisionally dissociated in the second stage of pumping. Therefore, all HCl was detected as Cl^-. Following collisional dissociation, the ion beam is further focused by a second RF-only quadrupole before entering the extraction optics for the time-of-flight (TOF) mass analyzer. The extraction frequency of the TOF was held at 66 kHz during CalNex, permitting measurement of organic and inorganic acids with mass-charge ratios between −10 and −200 m/Q. Raw spectra were subsequently time averaged and saved at 2 Hz.

HCl calibrations were conducted in the field using a calibrated HCl permeation source (VICI Metronics). The permeation source was calibrated in the laboratory following the CalNex deployment by trapping the effluent in an alkaline water matrix for subsequent analysis via ion chromatography (Metrohm ion chromatograph, single column, and chemical suppression). The permeation rate was measured to be 17 ± 2 ng min^{-1} at 50°C. The permeation source was housed in a custom-machined aluminum block, temperature controlled to 50°C, with ± 0.1°C precision. UHP N_2 was continuously passed over the permeation source and was subsequently further diluted with N_2 to achieve a constant mixing ratio of 1.1 ppb HCl that was added to the tip of the heated CalNex inlet. Calibrations were conducted every 90 min for

a total of 293 calibrations during the campaign. Background determinations were conducted every 30 min by overflowing the inlet with UHP N_2 (882 total).

In what follows, we first discuss the CI-TOFMS and the factors that contribute to the accuracy and precision of the instrument. We then discuss factors that contribute to systematic biases that may be imposed by the CalNex inlet design. The campaign average sensitivity, as determined through both direct calibrations and standard additions, was 104 ± 66 Hz ppt^{-1}, a factor of 3 lower than our previously reported sensitivity to formic acid (338 Hz ppt^{-1}) [*Bertram et al.*, 2011]. This decreased sensitivity toward HCl, relative to formic acid, is likely due to a combination of the relative transmission of the two acids through the inlet manifold (discussed below) coupled with the mass-dependent ion duty cycle that limits sensitivity at low m/Q [*Guilhaus et al.*, 2000]. Assuming that random uncertainty in the observed counts follows Poisson statistics, the limit of detection for HCl can be calculated using equation (E1), where c_f is the calibration factor, $[X]$ is the mixing ratio, B is the background count rate, and t is the integration time [*Bertram et al.*, 2011; *Wood et al.*, 2003].

$$\frac{S}{N} = \frac{c_f[X]t}{\sqrt{c_f[X]t + 2Bt}} \tag{E1}$$

Using a calibration factor (c_f) of 104 Hz ppt^{-1}, an upper limit to the observed background count rate (B) of 1.3×10^5 ion s^{-1}, the detection limit for 60 s averages and a signal-to-noise of 3 is 2 pptv. The limit of detection as calculated using the 3σ variability in all of the measured background determinations performed during CalNex yields a detection limit of 97 pptv. For comparison, remote oceanic mixing ratios of HCl typically range from 100 to 300 pptv, while urban regions can range from 100 pptv to above 1 ppbv [*Graedel and Keene*, 1995], placing the detection limit during CalNex at the lower end of typical ambient HCl mixing ratios. Continuous measurement of the $H^{37}Cl$ to $H^{35}Cl$ ratio during CalNex revealed a ratio of 0.27 ± 0.04, lower than the expected isotopic ratio of 0.32. The consistency of the ratio over all sampled air masses and during HCl calibrations suggests that the deviation is instrumental rather than a contamination at either m/Q.

The high background count rate observed during CalNex is attributed to a steady flux of HCl in the reagent ion delivery line, emanating from either the liquid nitrogen dewar, the gas handling lines, or the walls of the ionizer itself. Due to the small electron capture cross section for acetic anhydride [*Cooper and Compton*, 1973], we expect that trace HCl was directly ionized in the polonium source resulting in a stable, high, Cl^- background. In experiments following CalNex, the addition of trace O_2 to the ionizer (<1%) resulted in a 2–3 order of magnitude reduction in the Cl^- background signal. The high Cl^- background observed on CalNex is hypothesized to be a result of the reaction of electrons with HCl adsorbed to the walls of the polonium ionizer that were quenched following the addition of O_2, which can serve to efficiently remove electrons prior to wall reactions.

As described to this point, uncertainty in the HCl calibration gas concentration (±10%) is the primary factor contributing to the absolute accuracy of the HCl measurement. However, the required use of an inlet on the R/V *Atlantis* introduces systematic bias in the measured HCl concentrations, resulting from (i) HCl repartitioning in our heated inlet (positive bias), (ii) acid displacement reactions occurring on the inlet walls (positive bias), and (iii) HCl loss to the inlet surfaces during transit to the detection axis (negative bias). In what follows, we constrain each of these terms using a combination of in-field diagnostics, post-campaign experiments, and thermodynamic models.

To assess the impact of HCl volatilization from chloride-containing particles entrained into the sampling inlet on our measured HCl (g) signal, we use the Extended Aerosol Inorganics Model (E-AIM) Aerosol Thermodynamic Model (version IV). Specifically, we initialize the model with median temperature (288 K), RH (83%), and gas and aerosol chemical composition and calculate the resulting HCl and pCl^- for ambient conditions. We then change the temperature to 308 K, the temperature of our inlet, calculate the corresponding change in RH, and then calculate the percent change in HCl relative to the 288 K case using E-AIM. This method is used to estimate the potential systematic bias in our observations stemming from HCl repartitioning. For the median conditions encountered on CalNex, inlet HCl repartitioning results in a +10% systematic positive bias in the measurement with a range of <10% to 28% expected for the range of RH values observed (23% to 97%). We use in-field standard additions of HNO_3 to the inlet to assess the role of acid displacement reactions occurring on the inlet walls in biasing our HCl measurements. The inlet was changed either every second day or when the HNO_3 additions led to HCl production in the inlet, leading to greater than 20% increase in HCl signal. As such, it is estimated that acid displacement reactions occurring on the CalNex inlet result in a +20%

systematic positive bias in the measurement (conservative upper estimate). Measurement of HCl transmission efficiency both during CalNex and post campaign, as determined via standard addition of HCl to the inlet, ranged between 77% transmission at relative humidity less than 5% and 45% transmission for RH = 80%. However, given that the calibration gas (during both standard additions and calibrations) also traveled the length of the inlet, direct correction of our measurements using the laboratory-derived transmission efficiency would further bias the reported mixing ratios. As such, in what follows, we do not correct the HCl observations based on the three systematic biases reported here but rather use these diagnostic tools to bracket our certainty in the retrieved concentrations. Collectively, the systematic biases reported here amount to a conservative estimate to the uncertainty in the reported HCl measurement of +30% and −55%. Since CalNex, the inlet has been redesigned, using a high-flow (10 sLpm), low-pressure (200 mbar) heated inlet that permits HCl transmission greater than 95% at 80% RH.

2.3. Concurrent Measurements

NO_x and NO_y measurements were made using photolysis and Au-tube conversion (325°C, H_2), respectively, each followed by O_3 chemiluminescence at 1 Hz averaged to 1 min [*Williams et al.*, 2009]. NO_z was calculated as the difference between NO_y and NO_x ($NO_z \equiv NO_y - NO_x$). All gas phase measurements were averaged to 1 min time scales and filtered to remove self-sampling of the R/V *Atlantis* ship exhaust by using relative wind direction (−67.5° to 67.5°, measured by a wind vane anemometer). Data were also removed when the relative wind speed was <0.5 m s^{-1} as ship air was likely sampled rather than ambient air.

A two-stage multijet cascade impactor [*Berner et al.*, 1979] sampled submicrometer (<1 μm) and supermicrometer (>1 μm and <10 μm at 60% RH) particles at variable sampling intervals between 2 and 13 h. Extracts were analyzed on board using ion chromatography (IC) to determine ion concentrations, including particulate chloride (pCl^-), sodium (pNa^+), and magnesium (pMg^{2+}) as well as particulate sulfate (SO_4^{2-}), ammonium (NH_4^+), and nitrate (NO_3^-) [*Quinn et al.*, 2000] and reported at 25°C, 1013.25 mbar with an uncertainty of ±10%. However, as pCl^- is dependent on the liquid water content of the particle, drying of the particle (from a mean value of 83% in the ambient air to 60%) may result in a loss of pCl^- via volatilization of HCl. Therefore, the pCl^- concentrations reported should be considered lower limits.

2.4. Particulate Chloride Deficits

Comparisons of pCl^- and pNa^+ ratios in fresh sea spray and surface seawater have been investigated previously and are shown to be conserved. Molar ratios of pCl^- and pNa^+ are reported to be 1.165 in fresh sea spray [*Millero and Leung*, 1976; *Wilson*, 1975]. Considering that pNa^+ is a conservative tracer of sea salt, the amount of pCl^- in fresh sea spray ($ssCl^-$) can be calculated using the following equation:

$$ssCl^- = pNa^+ \times 1.165 \tag{E2}$$

where pNa^+ is the measured particulate sodium molar concentration [*Keene et al.*, 1986]. Therefore, the absolute chloride depleted from sea spray particle (d_{Cl}) and the fraction of chloride lost from the aerosol population ($f_{Cl\ lost}$) can be determined using equations (E3) and (E4), respectively.

$$d_{Cl} = ssCl^- - pCl^- \tag{E3}$$

$$f_{Cl\ lost} = \frac{d_{Cl}}{ssCl^-} \tag{E4}$$

For this analysis, d_{Cl} is converted to ppb equivalents for comparison to ambient HCl mixing ratios.

3. Results

During CalNex, large spatial differences in the HCl signal were observed. HCl mixing ratios were highest in the SC region, ranging from 0 to 16 ppb with a median mixing ratio of 1.3 ppb (interquartile range: 0.5–32.7 ppb) and a mean of 2.2 ± 2.3 ppb (1σ), as expected, due to the sampling of a series of outflow events from the Los Angeles basin coupled with high pCl^- concentrations. The mixing ratio of HCl in the NC region ranged from 0 to 1.9 ppb (median: 0.19 ppb and interquartile range: 0.10–0.38 ppb) with a mean of 0.27 ± 0.22 ppb (1σ). The observed mean mixing ratios are within the range of previous measurements in similar regions [*Graedel and Keene*, 1995; *Keene et al.*, 2007; *von Glasow and Crutzen*, 2003], while maximum HCl mixing ratios in SC are

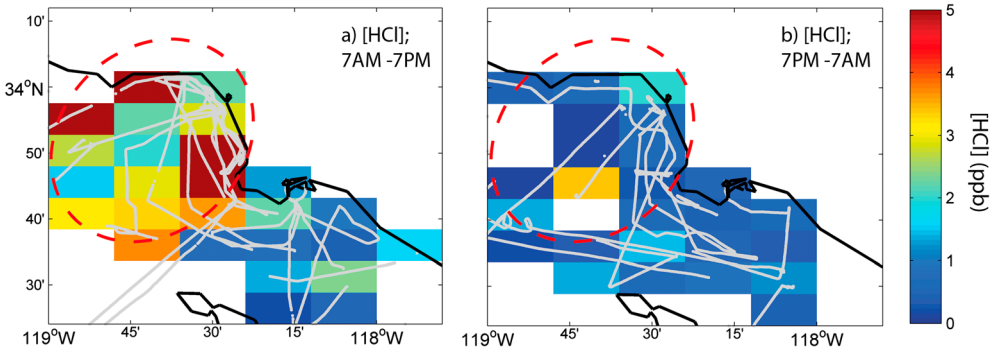

Figure 2. Binned (~5 km × 5 km) median HCl mixing ratios during day ((a) 7 A.M.–7 P.M. local time) and night ((b) 7 P.M.–7 A.M. local time) as observed in the Southern California sampling region. The red circles indicate a region where outflow was sampled. The R/V *Atlantis* ship track is shown in gray.

among the highest observed in polluted marine regions. In the following sections, we discuss the spatiotemporal variability in the SC sampling region during CalNex.

3.1. Spatial Variability in HCl in Coastal Southern California

Given the short atmospheric lifetime for HCl in the marine boundary layer (1–2 days), strong heterogeneity in the sources of HCl, and the well-characterized land-sea breeze circulation in coastal California [*Bao et al.*, 2008; *Langford et al.*, 2010; *Lu and Turco*, 1994, 1995], we expect significant spatiotemporal variability in HCl mixing ratios in the CalNex observations. To assess the strong spatial variability in the HCl measurements in coastal Southern California, observations made between 119° and 117.75°W and 33.3° and 34.2°N were binned into sixty 5 km × 5 km bins. Binned median HCl observations, shown in Figure 2, were further separated by time of day. Daytime mixing ratios of HCl (7 A.M. to 7 P.M., local time) routinely exceeded 5 ppb (Figure 2a), most notably in the primary region of the outflow of the Los Angeles Air Basin, while nighttime HCl mixing ratios

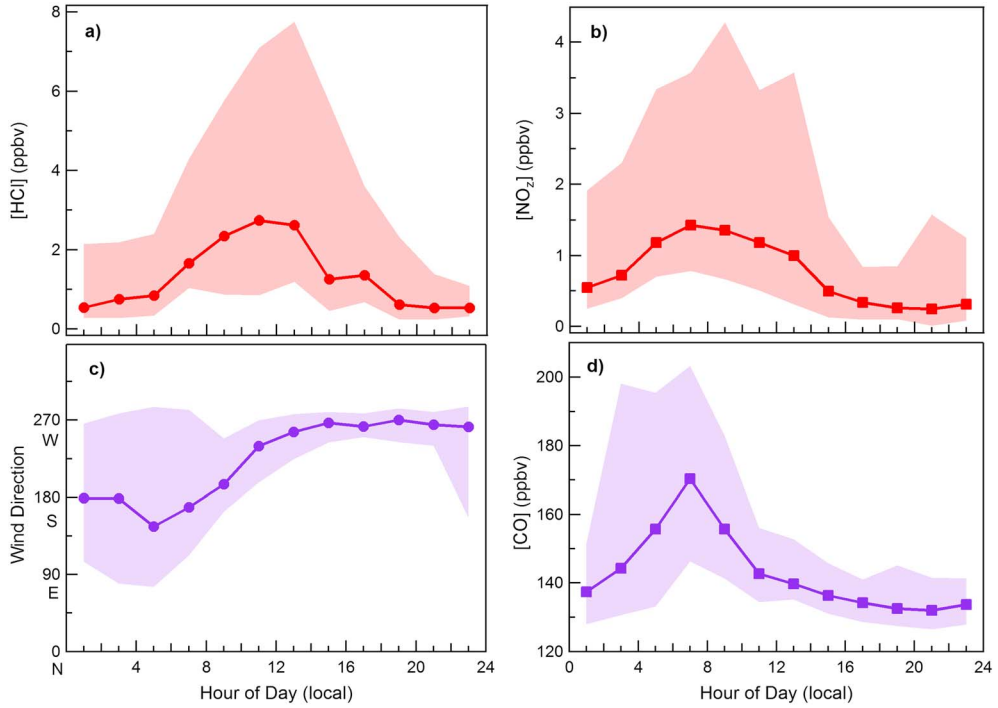

Figure 3. (a) Median HCl mixing ratio (red circles), (b) NO_z ($NO_z \equiv NO_y - NO_x$) mixing ratio (red squares), (c) wind direction (purple circles), and (d) carbon monoxide (CO) (purple squares) as measured in the Southern California sampling region. The shaded regions depict the interquartile range.

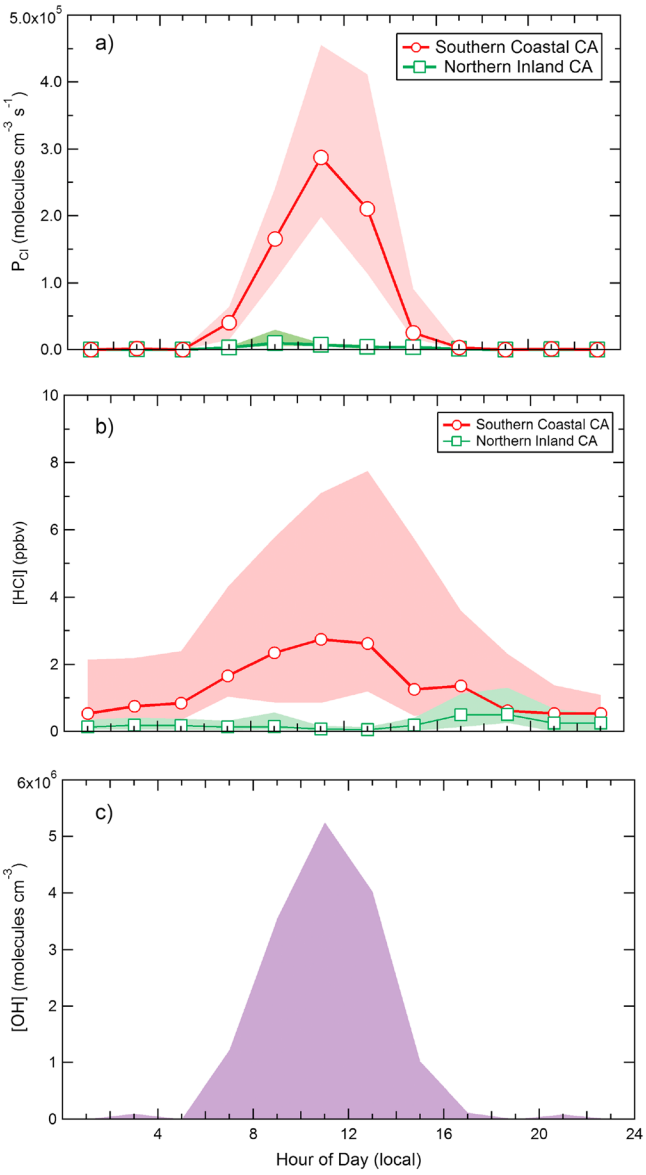

Figure 4. (a) Instantaneous Cl atom production rate (P_{Cl}) as calculated from (b) median HCl observations in the Northern (green) and Southern (red) California sampling regions and (c) modeled diel OH concentrations. The shaded region represents the interquartile range.

were consistently below 3 ppb (Figure 2b). This day-night variability may either be a result of diel changes in meteorological conditions and/or photochemical production mechanisms.

3.2. Temporal Distribution of HCl in Coastal Southern California

Figures 3a–3b depict the median bihourly mixing ratios of HCl and NO_z measured in SC. NO_z is used as an upper limit for the nitric acid (HNO_3) mixing ratio as our CI-TOFMS was not configured during CalNex to make quantitative measurements of HNO_3. HCl mixing ratios indicate a clear diel profile peaking at 11 A.M. The amplitude and hour of the peak mixing ratio varied slightly from day to day due to spatial variability in HCl mixing ratios and the R/V *Atlantis* sampling location and objectives. In contrast, the NO_z mixing ratio peaked at 8 A.M., much earlier than expected based solely on a photochemical HNO_3 production mechanism, suggesting that the following may be important in describing the diel behavior of HNO_3: (1) correlation with the temporal profile in wind direction, driven by land-sea breeze circulation, (2) the R/V *Atlantis* sampling bias toward making coastal measurements during morning hours, leading to higher NO_z mixing ratios in the morning near urban coastal areas and lower NO_z mixing ratios in the afternoon while sampling clean marine air, (3) reactive uptake of HNO_3 to sea spray aerosol that is competitive with the production of HNO_3, therefore removing HNO_3 as soon as it is produced, and/or (4) nitrogen oxides other than HNO_3 contribute to NO_z, causing the peak in the diel cycle to correspond with the production of other reactive nitrogen oxide species. To assess the role of meteorology in influencing the diel profile of HCl and NO_z, the diel profile of the wind direction in the SC region is shown in Figure 3c. These observations confirm that, on average, the wind was blowing offshore during the morning hours during peak NO_z concentrations and onshore through much of the late morning, afternoon, and evening, similar to the profile observed by *Lu and Turco* [1995], where the sea breeze began to blow onshore at 11:00 A.M. local time and continued into the evening [*Jacob*, 1999; *Lu and Turco*, 1994]. This is supported by the diel profile in carbon monoxide (CO) shown in Figure 3d. The CO profile peaks in the morning while offshore winds were being sampled and decreases at 11 A.M. as the wind shifts and clean marine air pushes onto the coast. The lower CO level persists through the evening as the wind continues to move onshore.

The observed time delay between peak NO_z and HCl mixing ratios, 7 A.M. and 11 A.M., respectively, has been observed in previous studies [*Graedel and Keene*, 1995; *John et al.*, 1988] and could be indicative of

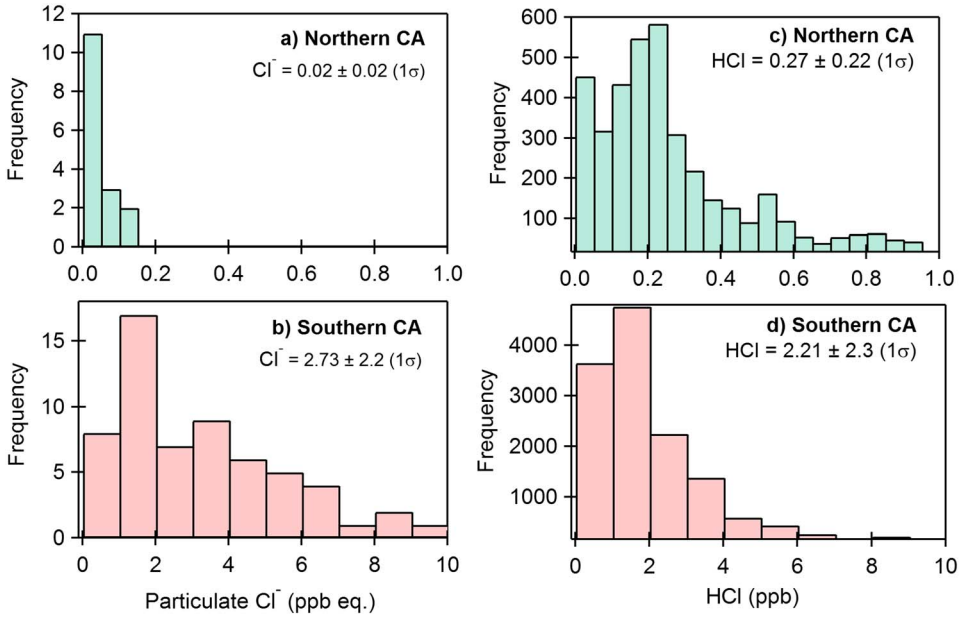

Figure 5. Observed frequency distribution of particulate chloride concentrations and HCl mixing ratio in the (a, c) Northern and (b, d) Southern California sampling regions.

thetime scale required for HCl production from HNO_3 acid displacement reactions, highlighting the role of secondary HCl production. As shown in Figure 3b, the NO_z profile broadens from 7 A.M. to midday, potentially masking two distinct peaks at 7 A.M. and solar noon, coinciding with offshore flow as determined by CO and peak OH concentrations, respectively. In contrast, HCl measurements peak near 11 A.M.

3.3. Chlorine Atom Production

The production rate of Cl atoms was calculated (Figure 4a) from the median HCl time series for both the Northern and Southern California sampling regions (Figure 4b), assuming that the reaction of HCl with OH is the only significant reaction pathway converting HCl to Cl atoms. Since the OH measurements were not made aboard the R/V *Atlantis* during CalNex, OH concentrations were modeled (Figure 4c). The average O_3 photolysis rates were measured aboard the R/V *Atlantis* using a filter radiometer [*Stark et al*., 2007] and were used to parameterize $O(^1D)$ [*Seinfeld and Pandis*, 2006] with the loss constrained by the observed mixing ratios of speciated volatile organic compounds, including methane, short chain alkanes (ethane, butane, pentane, and propane), and short chain alkenes (butene, propylene, and ethylene) [*Kuster et al*., 2003; *Riedel et al*., 2012]. The modeled OH concentration peaks at 5.3×10^6 molecules cm^{-3} with a $[OH]_{avg}$ of 1.3×10^6 molecules cm^{-3}, which is in agreement with previous studies for the SC sampling region [*Riedel et al*., 2012]. The instantaneous Cl atom production rate peaks at 2.9×10^5 molecules cm^{-3} s^{-1} (12:00), and the 24 h average Cl atom production rate was calculated to be 6.1×10^4 molecules cm^{-3} s^{-1} for this region. In contrast, the Cl atom production peaks at 9.9×10^3 molecules cm^{-3} s^{-1} (12:00), and the 24 h average Cl atom production rate was calculated to be 2.5×10^3 molecules cm^{-3} s^{-1} for the NC sampling regime. Other studies of Cl atom production rates in polluted and marine regions have reported a range in values from 4×10^3 to 4×10^6 molecules cm^{-3} s^{-1} for $ClNO_2$ and Cl_2 [*Finlayson-Pitts*, 1993; *Ganske et al*., 1992]. Recently, Riedel and coauthors utilized a Master Chemical Model to model the Cl atom production from a HCl, $ClNO_2$, and other Cl-containing species in the Los Angeles outflow region and calculated a maximum Cl atom production rate of 0.5×10^6 atoms cm^{-3} s^{-1} at noon for the "without-$ClNO_2$" scenario, of which HCl is the dominant source. Conversely, the "with-$ClNO_2$" scenario resulted in a maximum Cl atom production rate at 7 A.M. of 3.4×10^6 atoms cm^{-3} s^{-1}, which corresponds to the maximum contribution via $ClNO_2$ photolysis [*Riedel et al*., 2013].

3.4. Sea Spray Aerosol Dechlorination

The frequency distribution for HCl observations, as measured in both NC and SC are presented in Figures 5c and 5d. The mean observed HCl mixing ratio in NC was 0.27 ± 0.22 (1σ) ppb (median: 0.19 and interquartile range

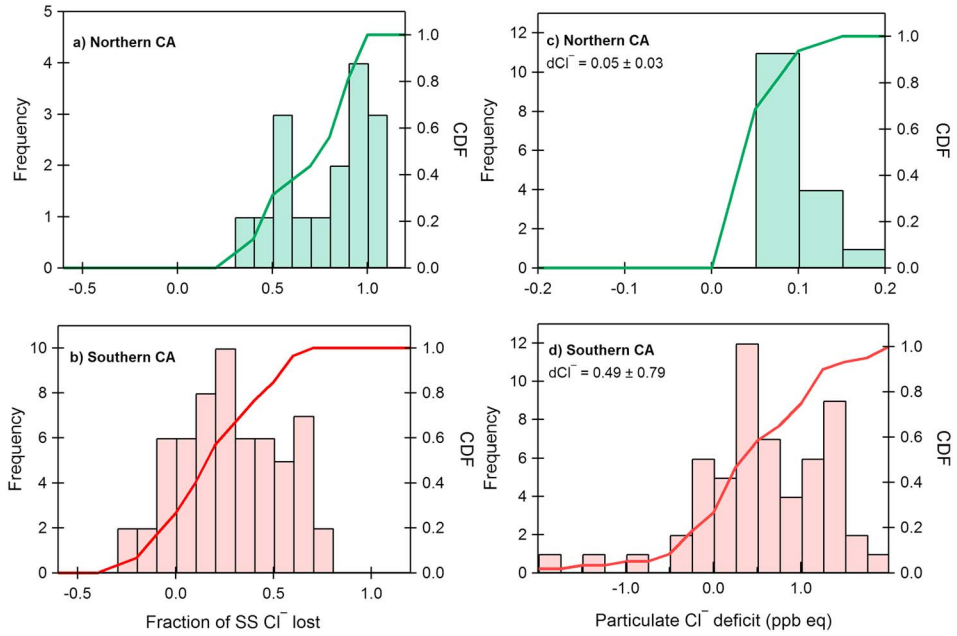

Figure 6. The frequency distribution of the calculated fraction of particulate chloride removed from sea spray particles in the (a) Northern and (b) Southern California sampling regions and (c, d) the calculated particulate chloride deficit in ppb equivalent for the entire particle size range (<1 μm to 10 μm). The cumulative distribution function for each distribution is also included on the right axis.

(iqr): 0.10–0.38 ppb), as compared to 2.2 ± 2.3 (1σ) ppb (median: 1.3 and iqr: 0.53–2.7 ppb) for the SC region. For comparison, the mean observed NO_z mixing ratio was 0.17 ± 6.0 (1σ) ppb (median: 0.43 and iqr: 0.29–0.59 ppb) and 2.3 ± 22 (1σ) ppb (median: 0.62 and iqr: 0.28–1.6 ppb) for the NC and SC regions, respectively. As mentioned in section 3, lower HCl mixing ratios in the NC region reflect a larger fraction of sampling time spent inland along the Sacramento River, where pCl^- concentrations are expected to be lower. The fraction of sea-salt Cl^- that has been lost from the aerosol population ($f_{Cl\ lost}$; submicrometer and supermicrometer) and the particle Cl^- deficit (d_{Cl}) were calculated via (E3) and (E4), respectively [*Laskin et al.*, 2012].

As shown in Figure 6a, sea spray aerosol Cl^- is heavily depleted in NC, with all samples exhibiting net depletion of Cl^-. This corresponds to a mean pCl^- deficit of 0.05 ± 0.03 (1σ) ppb. Assuming HCl (g) and pCl^- have similar lifetimes, an upper limit for the net HCl produced via dechlorination reactions from the sampled particle population (Figure 6c) can be determined. Figures 6b and 6d depict $f_{Cl\ lost}$ and d_{Cl} for the SC sampling region. In contrast to the NC samples, over 25% of SC samples indicate no net pCl^- depletion but rather an addition of Cl^- to the particle population. In the SC sampling region, our measurements indicate a mean pCl^- deficit of 0.49 ± 0.79 (1σ) ppb, small compared with the mean HCl mixing ratio of 2.1 ± 2.3 (1σ) ppb. In a closed system, where $\tau_{HCl} = \tau_{pCl-}$, this would suggest that sources other than sea-salt aerosol are required to sustain this disparity.

Previous measurements have shown Cl^- depletion to be more significant on submicrometer particles than supermicrometer particles [*Kerminen et al.*, 2000; *McInnes et al.*, 1994]. This observation has been attributed to (1) lower surface to volume ratio and/or diffusive limitations for heterogeneous and multiphase reactions occurring on supermicrometer particles, (2) shorter atmospheric lifetime of supermicrometer particles as compared with submicrometer particles, and (3) differences in particle liquid water content and particle pH [*Fridlind and Jacobson*, 2000; *Keene et al.*, 1998]. Figures 7a and 7b depict cumulative distribution functions (CDFs) of $f_{Cl\ lost}$ and d_{Cl} for submicrometer and supermicrometer particles separately as measured in the Southern California sampling region during all of CalNex. The observations indicate that submicrometer particles are more depleted in Cl^- (Figure 7a) than supermicrometer particles. However, the concentration of Cl^- depleted from the particle is higher in the supermicron mode as expected since the majority of the Cl^- mass exists in the supermicrometer mode (Figure 7b; pCl^- (d_p >1 μm)/ total pCl^- = 0.94 ± 0.11).

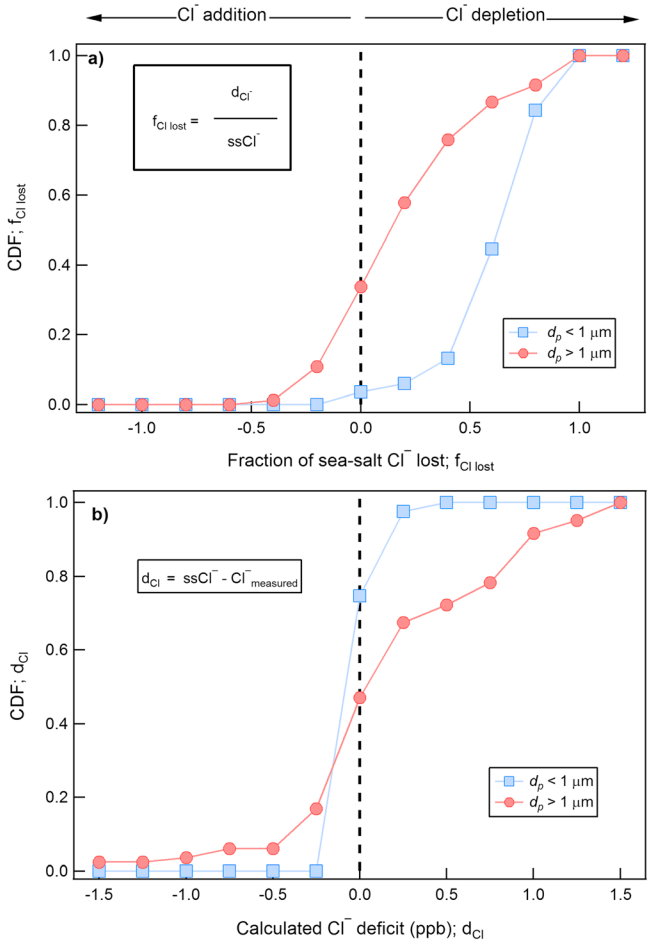

Figure 7. (a) Cumulative distribution function (CDF) of the fraction of chloride removed from submicrometer (blue squares) and supermicrometer (red circles) particles in Southern California sampling region. (b) CDF of the calculated chloride deficit (in ppb) for submicrometer (blue squares) and supermicrometer (red circles) particles in the Southern California sampling region.

3.5. Gas-Particle Partitioning of HCl

Calculation of the partitioning of HCl between the gas and aerosol phases for the average conditions in the Northern and Southern California sampling regions was conducted using the Extended Aerosol Inorganic Model (E-AIM) Aerosol Thermodynamic Model IV and constrained by the mean observations of gas- and particulate-phase chemical composition (including Na^+, NH_4^+, Cl^-, NO_3^-, and SO_4^{2-}) in addition to relative humidity in each region. The initial cation input was increased by less than 10% by combining Mg^{2+} concentrations to Na^+ and thereby obtaining charge balance. The equilibrium calculations resulted in submicrometer and supermicrometer HCl/pCl^- ratios (in mol/mol) of 78.3 and 10.7, respectively, for the NC sampling region. Calculated HCl/pCl^- ratios were within 33% and 9% of the observed ratios for the submicrometer and supermicrometer size ranges, respectively. In SC, the calculated HCl/pCl^- ratios for submicrometer and supermicrometer particles were 26.9 and 0.92. These ratios are within 2% (submicrometer) and 1% (supermicrometer) of the HCl/pCl^- ratio observed in the ambient data. *Keene et al.* [2007] observed a HCl/pCl^- ratio of 12.7 for all particles off the coast of Maine. For comparison, a ratio of 10.7 was observed during CalNex, within 20% of the observations in Maine. In both the submicrometer scenarios for SC and NC regions, the pH of the aerosol was calculated to be 2 and 2.7, respectively, which is consistent with previous particle acidity studies [*Fridlind and Jacobson*, 2000; *Keene et al.*, 2004]. While the SC supermicrometer analysis suggests a pH of 3.4, the NC supermicrometer particles indicate a pH of 7.1, higher than the pH range (2–6) observed in some previous observations and models [*Fridlind and Jacobson*, 2000; *Keene et al.*, 2004]. A pH of this alkalinity would result in a net loss in HCl, which is unlikely, as no Cl^- addition was observed in this region. The slightly alkaline pH calculated for supermicrometer particles might be an artifact of the uncertainty in the measurement as well as the calculation. Estimating pH has inherent uncertainty due to the limitations of the model (e.g., assumption of thermodynamic equilibrium, estimation of dissociation constants for strong acids, etc.) and the averaging of data over long sampling periods and an extensive sampling region; all of which are compounded by the uncertainty in the measurements [*Keene et al.*, 1998; *Young et al.*, 2013].

3.6. Primary HCl Emissions in Northern California

Here we describe a subset of the CalNex observations taken along the Sacramento River. These observations provide a unique opportunity to sample air that has variable amounts of marine influence in addition to a number of industrial facilities, including West Contra Landfill, Dow Chemical Company, and Conoco Phillips Refining Company. HCl emission rates for West Contra Landfill and Dow Chemical Company are estimated in

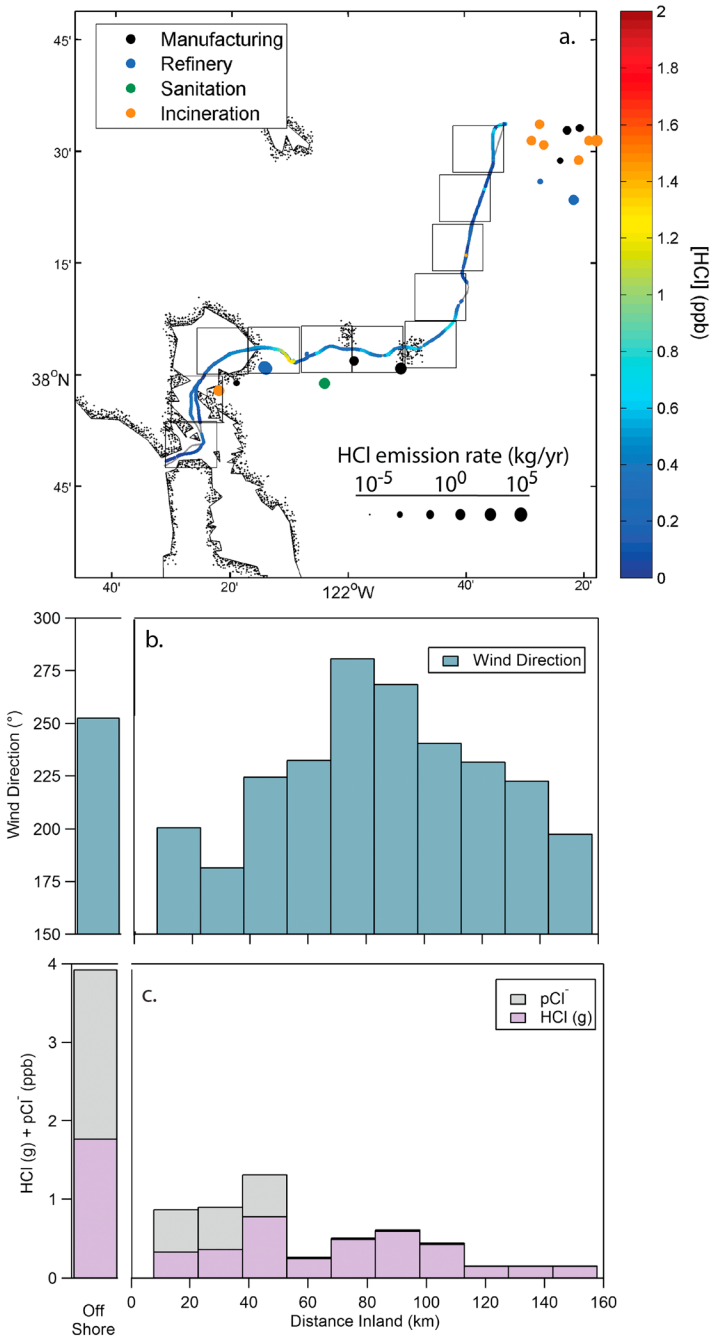

Figure 8. (a) The R/V *Atlantis* ship track along the Sacramento River in Northern California colored by HCl mixing ratio. Colored circles depict primary HCl sources in Northern California as defined by the California Emissions Inventory Development and Reporting System (CEIDARS Database). The color and size of the circle represents the source type and HCl emission rate, respectively. Gray boxes indicate the bin sizes (15 × 15 km) used to bin the observations. (b and c) Binned wind direction and mixing ratios of HCl and particulate chloride (pCl^-) observed in this region are shown as a function of distance inland.

the ARB inventory to be 3.65×10^{-6} and 1.80×10^{-5} Tg HCl yr^{-1}, respectively, with the Conoco Phillips Refining facility having the largest emission rate of 4.30×10^{-5} Tg HCl yr^{-1}. Between 4 and 6 June 2010, the R/V *Atlantis* traveled through the Carquinez Strait, sampling each of these isolated emissions sources (Figure 8a). Due to consistent westerly winds (230° ± 46° (1σ) and 4.5 ± 3.0 (1σ) m s^{-1}) encountered during our transect of the San Francisco Bay, as shown in Figure 8b, Carquinez Strait, and Sacramento River, the observations can to first order be discussed within a Lagrangian model framework, where we sampled a

marine air mass that progressed through the San Francisco Bay toward Sacramento. Figure 8c depicts binned pCl^- and HCl observations as a function of distance from the coastline along the Sacramento River. Here we focus on the sum of HCl (g) and pCl^-, as diel variations in oxidant loadings, temperature, and particle acidity complicate the interpretation of HCl or pCl^- independently. The sum of HCl (g) and pCl^- (hereafter ΣCl) are at a maximum directly offshore of the San Francisco Bay, reaching a combined mixing ratio of 3.9 ppb. As the R/V *Atlantis* proceeded under the Golden Gate Bridge and into the San Francisco Bay, ΣCl dropped rapidly to 0.88 ppbv.

4. Discussion

Current global reactive chlorine emission inventories estimate that greater than 80% of total tropospheric HCl production stems from particle dechlorination reactions [*Keene et al*., 1999]. Anthropogenic HCl emissions are expected to be highly variable spatially and have not been adequately constrained by observations, thus limiting our understanding of the impact of chlorine catalyzed chemistry, especially in continental regions [*Faxon and Allen*, 2013; *Thornton et al*., 2010]. In the following section we explore the relative source strengths for HCl from sea spray dechlorination reactions and direct emission to the atmosphere using both aerosol chloride and gas phase HCl observations in the Northern and Southern California sampling regions.

The NC and SC sampling regions represent two different regimes, influenced by varying levels of sea spray and urban outflow. The mixing ratio of NO_z in SC is significantly higher than the mixing ratio in NC, potentially due to more sampling time spent near polluted urban areas off the SC coast as compared with the Sacramento Delta. This outflow dependence is particularly highlighted in Figure 2 where elevated levels of HCl are observed primarily in the "outflow corridor" in the SC region. The lower availability of outflow containing HNO_3 and lower concentration of pCl^- in NC leads to a lower mixing ratio of HCl (max: 1.9 ppb) than that observed in the SC region (max: 16 ppb) and therefore results in differences in the Cl atom budget from HCl in these regions (Figure 4).

Observations of the pCl^- availability and corresponding HCl levels in the two regimes highlights potential differences in the production pathway for HCl between these regions. The SC region is characterized by a large range in HCl mixing ratios that are within the range of pCl^- mixing ratios measured (Figure 5). Conversely, the mixing ratios of HCl are significantly higher than the mixing ratios of pCl^- available in the NC region. This discrepancy between the HCl and pCl^- levels in the NC region may suggest the influence of HCl primary emissions sources, assuming that the lifetime of HCl is similar to the lifetime of the aerosol.

A large contribution of primary emissions to the HCl budget relative to sea spray dechlorination in NC may shift the equilibrium of HCl and pCl^- and the associated aerosol acidity. Though a net chloride deficit was observed in the SC region, the NC region contained an addition of chloride, particularly the submicrometer particles (Figure 7). Diminishing HCl volatilization and therefore the ability of a particle to buffer its acidity could lead to a suppression of the uptake of strong acids to the particle [*Keene et al*., 1998], affecting the pH of the multiphase system and the chlorine chemistry within the region. Though previous studies have suggested the influence of HCl point sources from comparisons of HCl and pCl^- deficits, many assume a similar lifetime of HCl and pCl^-. Often this is not the case, as larger particles, which are responsible for the majority of pCl^-, have short lifetimes in comparison with HCl. However, primary emissions of HCl are suspected to be influential, particularly in the Northern CA region, where known HCl point sources were downwind of the sampling platform. If the transect through the NC region is treated in a Lagrangian framework, in the absence of nonmarine sources for HCl or pCl^-, it is expected that ΣCl mixing ratios will decay with a time constant set by the lifetime of ΣCl. In contrast, our observations (Figure 8c) indicate the ΣCl increases as the R/V *Atlantis* proceeds through the Carquinez Strait toward Sacramento, while particulate Cl^- mixing ratios decrease from 0.3 ppb at the coastline to 0.09 ppb before the air mass leaves the San Francisco Bay (45 km), suggesting a potential role for nonmarine sources of HCl. However, the observed change in the ΣCl could also be a result of meteorological changes. Unfortunately, the ship's position and the general objectives of the CalNex campaign did not permit direct measurement of HCl emission ratios from these point sources, and therefore, the extent and significance of such emissions are beyond the limitations of this study. Nonetheless, our observations suggest that quantifying HCl emissions from point sources such as the refineries in the Carquinez Strait will be required to accurately model HCl and pCl^- concentrations in these

regions. Quantifying such emissions will provide constraints on the (1) HCl budget, (2) acidity of the multiphase system, and (3) chloride availability, particularly in inland regions, which has been of increasing interest as of late (e.g., $ClNO_2$ production from N_2O_5 chemistry).

5. Conclusions

Ship-based observations of gas phase HCl, pCl^-, and NO_y in coastal California were made during CalNex 2010. Median mixing ratios of HCl were 1.3 ppb (interquartile range: 0.53–2.7 ppb) and 0.19 ppb (interquartile range: 0.10–0.38) for Southern and Northern California, respectively, with a maximum above 16 ppb. When compared to the available pCl^- for these regions, point emissions of HCl were shown to be a potentially large source of HCl, which are not accurately accounted for in current HCl emission inventories. Analysis of available inventories illustrates potentially significant discrepancies in the reported contribution of HCl primary emissions. Future studies are needed to expand the currently limited HCl database as well as better characterize HCl point sources and their contribution to the HCl and Cl atom budget, especially in continental regions where dechlorination pathways are limited. Quantification of HCl direct emissions will advance our understanding of the role of halogen activation processes, like those involving $ClNO_2$, in regional chemical transport models.

Acknowledgments

This research was supported by the National Science Foundation CAREER award to T.H.B. (grant AGS-1151430) and in part by the NOAA Health of the Atmosphere Program. The authors would like to thank the Woods Hole Oceanographic Institute and the crew of the R/V *Atlantis* for accommodating us and our science objectives during CalNex 2010. We are grateful to Kimberly Prather and Elizabeth Fitzgerald for their assistance with IC analysis for determining permeation rates from our calibration sources. We also thank V. Agusiegbe at the California Air Resource Board for supplying us with HCl emissions data.

References

Agency, O. I. E (1992), *Energy Balances of OECD Countries, 1989-1990: Bilans Energetiques Des Pays De L'Ocde*, Renouf Publishing Company Limited, Ottawa, Canada.

Allan, W., D. C. Lowe, A. J. Gomez, H. Struthers, and G. W. Brailsford (2005), Interannual variation of 13C in tropospheric methane: Implications for a possible atomic chlorine sink in the marine boundary layer, *J. Geophys. Res.*, *110*, D11306, doi:10.1029/2004JD005650.

Allegrini, I., F. Santis, A. Febo, A. Liberti, and M. Possanzini (1984), Evaluation of atmospheric acidity—Sampling and analytical techniques, in *Physico-Chemical Behaviour of Atmospheric Pollutants*, edited by B. Versino and G. Angeletti, pp. 12-19, Springer, Netherlands, doi:10.1007/978-94-009-6505-8_2.

Appel, B. R., Y. Tokiwa, V. Povard, and E. L. Kothny (1991), The measurement of atmospheric hydrochloric-acid in Southern California, *Atmos. Environ. Gen. Top.*, *25*(2), 525–527.

Bao, J. W., S. A. Michelson, P. O. G. Persson, I. V. Djalalova, and J. M. Wilczak (2008), Observed and WRF-simulated low-level winds in a high-ozone episode during the Central California ozone study, *J. Appl. Meteorol. Climatol.*, *47*(9), 2372–2394, doi:10.1175/2008JAMC1822.1.

Bari, A., V. Ferraro, L. R. Wilson, D. Luttinger, and L. Husain (2003), Measurements of gaseous HONO, HNO_3,SO_2, HCl, NH_3, particulate sulfate and PM2.5 in New York, NY, *Atmos. Environ.*, *37*(20), 2825–2835, doi:10.1016/S1352-2310(03)00199-7.

Berner, A., C. Lürzer, F. Pohl, O. Preining, and P. Wagner (1979), The size distribution of the urban aerosol in Vienna, *Sci. Total Environ.*, *13*(3), 245–261, doi:10.1016/0048-9697(79)90105-0.

Bertram, T. H., J. R. Kimmel, T. A. Crisp, O. S. Ryder, R. L. N. Yatavelli, J. A. Thornton, M. J. Cubison, M. Gonin, and D. R. Worsnop (2011), A field-deployable, chemical ionization time-of-flight mass spectrometer, *Atmos. Meas. Tech.*, *4*(7), 1471–1479, doi:10.5194/amt-4-1471-2011.

Brown, S. S., and J. Stutz (2012), Nighttime radical observations and chemistry, *Chem. Soc. Rev.*, *41*(19), 6405–6447, doi:10.1039/C2CS35181A.

Cooper, C. D., and R. N. Compton (1973), Electron attachment to cyclic anhydrides and related compounds, *J. Chem. Phys.*, *59*(7), 3550–3565, doi:10.1063/1.1680519.

Dasgupta, P. K., S. W. Campbell, R. S. Al-Horr, S. M. R. Ullah, J. Z. Li, C. Amalfitano, and N. D. Poor (2007), Conversion of sea salt aerosol to NaNO (3) and the production of HCl: Analysis of temporal behavior of aerosol chloride/nitrate and gaseous HCl/HNO(3) concentrations with AIM, *Atmos. Environ.*, *41*(20), 4242–4257, doi:10.1016/j.atmosenv.2006.09.054.

Dimmock, N. A., and G. B. Marshall (1987), The determination of hydrogen-chloride in ambient air with diffusion denuder tubes, *Anal. Chim. Acta*, *202*, 49–59, doi:10.1016/S0003-2670(00)85901-2.

Eldering, A., P. A. Solomon, L. G. Salmon, T. Fall, and G. R. Cass (1991), Hydrochloric acid: A regional perspective on concentrations and formation in the atmosphere of Southern California, *Atmos. Environ. Gen. Top.*, *25*(10), 2091–2102, doi:10.1016/0960-1686(91)90086-M.

Erickson, D. J., C. Seuzaret, W. C. Keene, and S. L. Gong (1999), A general circulation model based calculation of HCl and $ClNO_2$ production from sea salt dechlorination: Reactive Chlorine Emissions Inventory, *J. Geophys. Res.*, *104*(D7), 8347–8372, doi:10.1029/98JD01384.

Erisman, J. W., A. W. M. Vermetten, W. A. H. Asman, A. Waijersijpelaan, and J. Slanina (1988), Vertical-distribution of gases and aerosols—The behavior of ammonia and related components in the lower atmosphere, *Atmos. Environ.*, *22*(6), 1153–1160, doi:10.1016/0004-6981(88)90345-9.

Faxon, C. B., and D. T. Allen (2013), Chlorine chemistry in urban atmospheres: A review, *Environ. Chem.*, *10*(3), 221–233, doi:10.1071/EN13026.

Finlayson-Pitts, B. J. (1993), Chlorine atoms as a potential tropospheric oxidant in the marine boundary layer, *Res. Chem. Intermed.*, *19*(3), 235–249, doi:10.1163/156856793X00091.

Finlayson-Pitts, B. J. (2009), Halogens in the troposphere, *Anal. Chem.*, *82*(3), 770–776, doi:10.1021/ac901478p.

Finlayson-Pitts, B. J., and J. N. Pitts (1999), *Chemistry of the Upper and Lower Atmosphere: Theory, Experiments, and Applications*, Science, Elsevier.

Fridlind, A. M., and M. Z. Jacobson (2000), A study of gas-aerosol equilibrium and aerosol pH in the remote marine boundary layer during the First Aerosol Characterization Experiment (ACE 1), *J. Geophys. Res.*, *105*(D13), 17,325–17,340, doi:10.1029/2000JD900209.

Ganske, J. A., H. N. Berko, and B. J. Finlayson-Pitts (1992), Absorption cross sections for gaseous $ClNO_2$ and Cl_2 at 298 K: Potential organic oxidant source in the marine troposphere, *J. Geophys. Res.*, *97*(D7), 7651–7656, doi:10.1029/92JD00414.

Gard, E. E., et al. (1998), Direct observation of heterogeneous chemistry in the atmosphere, *Science*, *279*(5354), 1184–1187, doi:10.1126/science.279.5354.1184.

Gounon, J., and A. Milhau (1986), Analysis of inorganic pollutants emitted by the city of Paris garbage incineration plants, *Waste Manage. Res.*, *4*(1), 95–104, doi:10.1177/0734242x8600400111.

Graedel, T. E., and W. C. Keene (1995), Tropospheric budget of reactive chlorine, *Global Biogeochem. Cycles*, *9*(1), 47–77, doi:10.1029/94GB03103.

Grosjean, D. (1990), Liquid-chromatography analysis of chloride and nitrate with negative ultraviolet detection: Ambient levels and relative abundance of gas-phase inorganic and organic-acids in Southern California, *Environ. Sci. Technol.*, *24*(1), 77–81, doi:10.1021/Es00071a007.

Guilhaus, M., D. Selby, and V. Mlynski (2000), Orthogonal acceleration time-of-flight mass spectrometry, *Mass Spectrom. Rev.*, *19*(2), 65–107, doi:10.1002/(SICI)1098-2787(2000)19:2<65:AID-MAS1>3.0.CO;2-E.

Harris, G. W., D. Klemp, and T. Zenker (1992), An upper limit on the HCl near-surface mixing-ratio over the Atlantic measured using TDLAS, *J. Atmos. Chem.*, *15*(3–4), 327–332, doi:10.1007/Bf00115402.

Harrison, R. M., and A. G. Allen (1990), Measurements of atmospheric HNO_3, HCl and associated species on a small network in eastern England, *Atmos. Environ. Gen. Top.*, *24*(2), 369–376, doi:10.1016/0960-1686(90)90116-5.

Iwasaki, Y., N. Yoshiharu, and N. Tanikawa (1985), High concentration of hydrogen chloride in the atmosphere, Tokyo-to Kogai Kankyusho Nenpo, 3–6, Tokyoto Kogai Kankyusho, Tokyo.

Jacob, D. J. (1999), *Introduction to Atmospheric Chemistry*, vol. xii, 266 pp., Princeton Univ. Press, Princeton, N. J.

John, W., S. M. Wall, and J. L. Ondo (1988), A new method for nitric acid and nitrate aerosol measurement using the dichotomous sampler, *Atmos. Environ.*, *22*(*8*), 1627–1635, doi:10.1016/0004-6981(88)90390-3.

Johnson, C. A., L. Sigg, and J. Zobrist (1987), Case studies on the chemical composition of fogwater: The influence of local gaseous emissions, *Atmos. Environ.*, *21*(11), 2365–2374, doi:10.1016/0004-6981(87)90371-4.

Jourdain, B., and M. Legrand (2002), Year-round records of bulk and size-segregated aerosol composition and HCl and HNO_3 levels in the Dumont d'Urville (coastal Antarctica) atmosphere: Implications for sea-salt aerosol fractionation in the winter and summer, *J. Geophys. Res.*, *107*(D22), 4645, doi:10.1029/2002JD002471.

Kajii, Y., H. Akimoto, Y. Komazaki, S. Tanaka, H. Mukai, K. Murano, and J. T. Merrill (1997), Long-range transport of ozone, carbon monoxide, and acidic trace gases at Oki Island, Japan, during PEM-West B PEACAMPOT B campaign, *J. Geophys. Res.*, *102*(D23), 28,637–28,649, doi:10.1029/97JD02013.

Kaneyasu, N., H. Yoshikado, T. Mizuno, K. Sakamoto, and M. Soufuku (1999), Chemical forms and sources of extremely high nitrate and chloride in winter aerosol pollution in the Kanto Plain of Japan, *Atmos. Environ.*, *33*(11), 1745–1756, doi:10.1016/S1352-2310(98)00396-3.

Keene, W. C., and D. L. Savoie (1998), The pH of deliquesced sea-salt aerosol in polluted marine air, *Geophys. Res. Lett.*, *25*(12), 2181–2184, doi:10.1029/98GL01591.

Keene, W. C., A. A. P. Pszenny, J. N. Galloway, and M. E. Hawley (1986), Sea-salt corrections and interpretation of constituent ratios in marine precipitation, *J. Geophys. Res.*, *91*(D6), 6647–6658, doi:10.1029/JD091iD06p06647.

Keene, W. C., A. A. P. Pszenny, D. J. Jacob, R. A. Duce, J. N. Galloway, J. J. Schultz-Tokos, H. Sievering, and J. F. Boatman (1990), The geochemical cycling of reactive chlorine through the marine troposphere, *Global Biogeochem. Cycles*, *4*(4), 407–430, doi:10.1029/GB004i004p00407.

Keene, W. C., R. Sander, A. A. P. Pszenny, R. Vogt, P. J. Crutzen, and J. N. Galloway (1998), Aerosol pH in the marine boundary layer: A review and model evaluation, *J. Aerosol Sci.*, *29*(3), 339–356, doi:10.1016/S0021-8502(97)10011-8.

Keene, W. C., et al. (1999), Composite global emissions of reactive chlorine from anthropogenic and natural sources: Reactive Chlorine Emissions Inventory, *J. Geophys. Res.*, *104*(D7), 8429–8440, doi:10.1029/1998JD100084.

Keene, W. C., A. A. P. Pszenny, J. R. Maben, E. Stevenson, and A. Wall (2004), Closure evaluation of size-resolved aerosol pH in the New England coastal atmosphere during summer, *J. Geophys. Res.*, *109*, D23307, doi:10.1029/2004JD004801.

Keene, W. C., R. M. Lobert, P. J. Crutzen, J. R. Maben, D. H. Scharffe, T. Landmann, C. Hely, and C. Brain (2006), Emissions of major gaseous and particulate species during experimental burns of southern African biomass, *J. Geophys. Res.*, *111*, D04301, doi:10.1029/2005JD006319.

Keene, W. C., J. Stutz, A. A. P. Pszenny, J. R. Maben, E. V. Fischer, A. M. Smith, R. von Glasow, S. Pechtl, B. C. Sive, and R. K. Varner (2007), Inorganic chlorine and bromine in coastal New England air during summer, *J. Geophys. Res.*, *112*, D10S12, doi:10.1029/2006JD007689.

Keene, W. C., M. S. Long, A. A. P. Pszenny, R. Sander, J. R. Maben, A. J. Wall, T. L. O'Halloran, A. Kerkweg, E. V. Fischer, and O. Schrems (2009), Latitudinal variation in the multiphase chemical processing of inorganic halogens and related species over the eastern North and South Atlantic Oceans, *Atmos. Chem. Phys.*, *9*(19), 7361–7385, doi:10.5194/acp-9-7361-2009.

Kerminen, V.-M., K. Teinilä, and R. Hillamo (2000), Chemistry of sea-salt particles in the summer Antarctic atmosphere, *Atmos. Environ.*, *34*(17), 2817–2825, doi:10.1016/S1352-2310(00)00089-3.

Keuken, M. P., C. A. M. Schoonebeek, A. Vanwensveenlouter, and J. Slanina (1988), Simultaneous sampling of NH_3, HNO_3, HCl, SO_2 and H_2O_2 in ambient air by a wet annular denuder system, *Atmos. Environ.*, *22*(11), 2541–2548, doi:10.1016/0004-6981(88)90486-6.

Khalil, M. A. K., R. M. Moore, D. B. Harper, J. M. Lobert, D. J. Erickson, V. Koropalov, W. T. Sturges, and W. C. Keene (1999), Natural emissions of chlorine-containing gases: Reactive Chlorine Emissions Inventory, *J. Geophys. Res.*, *104*(D7), 8333–8346, doi:10.1029/1998JD100079.

Kim, S., et al. (2008), Airborne measurements of HCl from the marine boundary layer to the lower stratosphere over the North Pacific Ocean during INTEX-B, *Atmos. Chem. Phys. Discuss.*, *8*(1), 3563–3595, doi:10.5194/acpd-8-3563-2008.

Knipping, E. M., and D. Dabdub (2002), Impact of chlorine emissions from sea-salt aerosol on coastal urban ozone, *Environ. Sci. Technol.*, *37*(2), 275–284, doi:10.1021/es025793z.

Kritz, M. A., and J. Rancher (1980), Circulation of Na, Cl, and Br in the tropical marine atmosphere, *J. Geophys. Res.*, *85*(C3), 1633–1639, doi:10.1029/Jc085ic03p01633.

Kuster, W. C., B. T. Jobson, T. Karl, D. Riemer, E. Apel, P. D. Goldan, and F. C. Fehsenfeld (2003), Intercomparison of volatile organic carbon measurement techniques and data at La Porte during the TexAQS2000 Air Quality Study, *Environ. Sci. Technol.*, *38*(1), 221–228, doi:10.1021/es034710r.

Langford, A. O., C. J. Senff, R. J. Alvarez, R. M. Banta, and R. M. Hardesty (2010), Long-range transport of ozone from the Los Angeles Basin: A case study, *Geophys. Res. Lett.*, *37*, L06807, doi:10.1029/2010GL042507.

Laskin, A., R. C. Moffet, M. K. Gilles, J. D. Fast, R. A. Zaveri, B. Wang, P. Nigge, and J. Shutthanandan (2012), Tropospheric chemistry of internally mixed sea salt and organic particles: Surprising reactivity of NaCl with weak organic acids, *J. Geophys. Res.*, *117*, D15302, doi:10.1029/2012JD017743.

Lawler, M. J., B. D. Finley, W. C. Keene, A. A. P. Pszenny, K. A. Read, R. von Glasow, and E. S. Saltzman (2009), Pollution-enhanced reactive chlorine chemistry in the eastern tropical Atlantic boundary layer, *Geophys. Res. Lett.*, *36*, L08810, doi:10.1029/2008GL036666.

Lawler, M. J., R. Sander, L. J. Carpenter, J. D. Lee, R. von Glasow, R. Sommariva, and E. S. Saltzman (2011), HOCl and Cl_2 observations in marine air, *Atmos. Chem. Phys.*, *11*(15), 7617–7628, doi:10.5194/acp-11-7617-2011.

Lindgren, P. F. (1992), Diffusion scrubber-ion chromatography for the measurement of trace levels of atmospheric HC1, *Atmos. Environ. Gen. Top.*, *26*(1), 43–49, doi:10.1016/0960-1686(92)90259-N.

Lobert, J. M., W. C. Keene, J. A. Logan, and R. Yevich (1999), Global chlorine emissions from biomass burning: Reactive Chlorine Emissions Inventory, *J. Geophys. Res.*, *104*(D7), 8373–8389, doi:10.1029/1998JD100077.

Lu, R., and R. P. Turco (1994), Air pollutant transport in a coastal environment. Part I: Two-dimensional simulations of sea-breeze and mountain effects, *J. Atmos. Sci.*, *51*(15), 2285–2308, doi:10.1175/1520-0469(1994)051<2285:APTIAC>2.0.CO;2.

Lu, R., and R. P. Turco (1995), Air pollutant transport in a coastal environment—II. Three-dimensional simulations over Los Angeles basin, *Atmos. Environ.*, *29*(13), 1499–1518, doi:10.1016/1352-2310(95)00015-Q.

Maben, J. R., W. C. Keene, A. A. P. Pszenny, and J. N. Galloway (1995), Volatile inorganic Cl in surface air over eastern North America, *Geophys. Res. Lett.*, *22*(24), 3513–3516, doi:10.1029/95GL03335.

Marche, P., A. Barbe, C. Secroun, J. Corr, and P. Jouve (1980), Ground based spectroscopic measurements of HCl, *Geophys. Res. Lett.*, *7*(11), 869–872, doi:10.1029/Gl007i011p00869.

Martinez, M., T. Arnold, and D. Perner (1999), The role of bromine and chlorine chemistry for arctic ozone depletion events in Ny-Ålesund and comparison with model calculations, *Ann. Geophys.*, *17*(7), 941–956, doi:10.1007/s00585-999-0941-4.

Matsumoto, M., and T. Okita (1998), Long term measurements of atmospheric gaseous and aerosol species using an annular denuder system in Nara, Japan, *Atmos. Environ.*, *32*(8), 1419–1425, doi:10.1016/S1352-2310(97)00270-7.

Matusca, P., B. Schwarz, and K. Bachmann (1984), Measurements of diurnal concentration variations of gaseous HCl in air in the subnanogram range, *Atmos. Environ.*, *18*(8), 1667–1675, doi:10.1016/0004-6981(84)90389-5.

McCulloch, A., M. L. Aucott, C. M. Benkovitz, T. E. Graedel, G. Kleiman, P. M. Midgley, and Y.-F. Li (1999), Global emissions of hydrogen chloride and chloromethane from coal combustion, incineration and industrial activities: Reactive Chlorine Emissions Inventory, *J. Geophys. Res.*, *104*(D7), 8391–8403, doi:10.1029/1999JD900025.

McInnes, L. M., D. S. Covert, P. K. Quinn, and M. S. Germani (1994), Measurements of chloride depletion and sulfur enrichment in individual sea-salt particles collected from the remote marine boundary layer, *J. Geophys. Res.*, *99*(D4), 8257–8268, doi:10.1029/93JD03453.

Millero, F. J., and W. H. Leung (1976), The thermodynamics of seawater at one atmosphere, *Am. J. Sci.*, *276*(9), 1035–1077, doi:10.2475/ajs.276.9.1035.

Neissner, R. (1981), Ein neuer Weg zur Bestimmung starker Säuren und ihrer Salze in der Atmosphäre, dissertation, Univ. Dortmund, Dortmund, Germany.

Osthoff, H. D., et al. (2008), High levels of nitryl chloride in the polluted subtropical marine boundary layer, *Nat. Geosci.*, *1*(5), 324–328, doi:10.1038/ngeo177.

Pechtl, S., and R. von Glasow (2007), Reactive chlorine in the marine boundary layer in the outflow of polluted continental air: A model study, *Geophys. Res. Lett.*, *34*, L11813, doi:10.1029/2007GL029761.

Platt, U., W. Allan, and D. Lowe (2004), Hemispheric average Cl atom concentration from 13C/12C ratios in atmospheric methane, *Atmos. Chem. Phys.*, *4*(9/10), 2393–2399, doi:10.5194/acp-4-2393-2004.

Pszenny, A. A. P., E. V. Fischer, R. S. Russo, B. C. Sive, and R. K. Varner (2007), Estimates of Cl atom concentrations and hydrocarbon kinetic reactivity in surface air at Appledore Island, Maine (USA), during International Consortium for Atmospheric Research on Transport and Transformation/Chemistry of Halogens at the Isles of Shoals, *J. Geophys. Res.*, *112*, D10S13, doi:10.1029/2006JD007725.

Pszenny, A. A. P., W. C. Keene, D. J. Jacob, S. Fan, J. R. Maben, M. P. Zetwo, M. Springer-Young, and J. N. Galloway (1993), Evidence of inorganic chlorine gases other than hydrogen chloride in marine surface air, *Geophys. Res. Lett.*, *20*(8), 699–702, doi:10.1029/93GL00047.

Pszenny, A. A. P., J. Moldanová, W. C. Keene, R. Sander, J. R. Maben, M. Martinez, P. J. Crutzen, D. Perner, and R. G. Prinn (2004), Halogen cycling and aerosol pH in the Hawaiian marine boundary layer, *Atmos. Chem. Phys.*, *4*(1), 147–168, doi:10.5194/acp-4-147-2004.

Puxbaum, H., E. Quintana, and M. Pimminger (1985), Spatial-distribution of atmospheric aerosol constituents in Linz (Austria), *Fresen. Z. Anal. Chem.*, *322*(2), 205–212, doi:10.1007/Bf00517660.

Quinn, P. K., et al. (2000), Surface submicron aerosol chemical composition: What fraction is not sulfate?, *J. Geophys. Res.*, *105*(D5), 6785–6805, doi:10.1029/1999JD901034.

Rahn, K. A., R. D. Borys, and R. A. Duce (1976), Tropospheric halogen gases: Inorganic and organic components, *Science*, *192*(4239), 549–550, doi:10.1126/science.192.4239.549.

Rahn, K. A., R. D. Borys, E. L. Butler, and R. A. Duce (1979), Gaseous and particulate halogens in the New York City atmosphere*, *Ann. N. Y. Acad. Sci.*, *322*(1), 143–151, doi:10.1111/j.1749-6632.1979.tb14123.x.

Riedel, T. P., et al. (2012), Nitryl chloride and molecular chlorine in the coastal marine boundary layer, *Environ. Sci. Technol.*, doi:10.1021/es204632r.

Riedel, T. P., et al. (2013), An MCM modeling study of nitryl chloride ($ClNO_2$) impacts on oxidation, ozone production and nitrogen oxide partitioning in polluted continental outflow, *Atmos. Chem. Phys. Discuss.*, *13*(11), 28,973–29,006, doi:10.5194/acpd-13-28973-2013.

Rudolph, J., B. Ramacher, C. Plass-DÜLmer, K. P. MÜLler, and R. Koppmann (1997), The indirect determination of chlorine atom concentration in the troposphere from changes in the patterns of non-methane hydrocarbons, *Tellus B*, *49*(5), 592–601, doi:10.1034/j.1600-0889.49.issue5.13.x.

Ryerson, T. B., et al. (2013), The 2010 California Research at the Nexus of Air Quality and Climate Change (CalNex) field study, *J. Geophys. Res. Atmos.*, *118*, 5830–5866, doi:10.1002/jgrd.50331.

Saiz-Lopez, A., and R. von Glasow (2012), Reactive halogen chemistry in the troposphere, *Chem. Soc. Rev.*, *41*(19), 6448–6472, doi:10.1039/C2CS35208G.

Sarwar, G., H. Simon, P. Bhave, and G. Yarwood (2012), Examining the impact of heterogeneous nitryl chloride production on air quality across the United States, *Atmos. Chem. Phys.*, *12*(14), 6455–6473, doi:10.5194/acp-12-6455-2012.

Seinfeld, J. H., and S. N. Pandis (2006), *Atmospheric Chemistry and Physics: From Air Pollution to Climate Change*, 2nd ed., vol. xxviii, 1203 pp., J. Wiley, Hoboken, N. J.

Singh, H. B., and J. F. Kasting (1988), Chlorine-hydrocarbon photochemistry in the marine troposphere and lower stratosphere, *J. Atmos. Chem.*, *7*(3), 261–285, doi:10.1007/BF00130933.

Singh, H. B., et al. (1996), Low ozone in the marine boundary layer of the tropical Pacific Ocean: Photochemical loss, chlorine atoms, and entrainment, *J. Geophys. Res.*, *101*(D1), 1907–1917, doi:10.1029/95JD01028.

Spicer, C. W. (1986), Patterns of atmospheric nitrates, sulfate, and hydrogen chloride in the central Ohio River Valley over a one-year period, *Environ. Int.*, *12*(5), 513–518, doi:10.1016/0160-4120(86)90145-5.

Stark, H., B. M. Lerner, R. Schmitt, R. Jakoubek, E. J. Williams, T. B. Ryerson, D. T. Sueper, D. D. Parrish, and F. C. Fehsenfeld (2007), Atmospheric in situ measurement of nitrate radical (NO_3) and other photolysis rates using spectroradiometry and filter radiometry, *J. Geophys. Res.*, *112*, D10S04, doi:10.1029/2006JD007578.

Sturges, W. T., and R. M. Harrison (1989), The use of nylon filters to collect HCl: Efficiencies, interferences and ambient concentrations, *Atmos. Environ.*, *23*(9), 1987–1996, doi:10.1016/0004-6981(89)90525-8.

Thornton, J. A., et al. (2010), A large atomic chlorine source inferred from mid-continental reactive nitrogen chemistry, *Nature*, *464*(7286), 271–274, doi:10.1038/nature08905.

Veres, P., J. M. Roberts, C. Warneke, D. Welsh-Bon, M. Zahniser, S. Herndon, R. Fall, and J. de Gouw (2008), Development of negative-ion proton-transfer chemical-ionization mass spectrometry (NI-PT-CIMS) for the measurement of gas-phase organic acids in the atmosphere, *Int. J. Mass Spectrom.*, *274*(1–3), 48–55, doi:10.1016/j.ijms.2008.04.032.

Vogt, R., P. J. Crutzen, and R. Sander (1996), A mechanism for halogen release from sea-salt aerosol in the remote marine boundary layer, *Nature*, *383*(6598), 327–330.

von Glasow, R., and P. J. Crutzen (2003), Tropospheric halogen, *Chemistry*, *1–67*, doi:10.1016/b0-08-043751-6/04141-4.

Watson, L. R., J. M. Van Doren, P. Davidovits, D. R. Worsnop, M. S. Zahniser, and C. E. Kolb (1990), Uptake of HCl molecules by aqueous sulfuric acid droplets as a function of acid concentration, *J. Geophys. Res.*, *95*(D5), 5631–5638, doi:10.1029/JD095iD05p05631.

Williams, E. J., B. M. Lerner, P. C. Murphy, S. C. Herndon, and M. S. Zahniser (2009), Emissions of NO_x, SO_2, CO, and HCHO from commercial marine shipping during Texas Air Quality Study (TexAQS) 2006, *J. Geophys. Res.*, *114*, D21306, doi:10.1029/2009JD012094.

Wilson, T. (1975), Salinity and major elements of sea water, in *Chemical Oceanography*, 2nd edn., vol. *1*, pp. 365-413, Academic Press, London, New York.

Wingenter, O. W., M. K. Kubo, N. J. Blake, T. W. Smith, D. R. Blake, and F. S. Rowland (1996), Hydrocarbon and halocarbon measurements as photochemical and dynamical indicators of atmospheric hydroxyl, atomic chlorine, and vertical mixing obtained during Lagrangian flights, *J. Geophys. Res.*, *101*(D2), 4331–4340, doi:10.1029/95JD02457.

Wingenter, O. W., D. R. Blake, N. J. Blake, B. C. Sive, F. S. Rowland, E. Atlas, and F. Flocke (1999), Tropospheric hydroxyl and atomic chlorine concentrations, and mixing timescales determined from hydrocarbon and halocarbon measurements made over the Southern Ocean, *J. Geophys. Res.*, *104*(D17), 21,819–21,828, doi:10.1029/1999JD900203.

Wingenter, O. W., B. C. Sive, N. J. Blake, D. R. Blake, and F. S. Rowland (2005), Atomic chlorine concentrations derived from ethane and hydroxyl measurements over the equatorial Pacific Ocean: Implication for dimethyl sulfide and bromine monoxide, *J. Geophys. Res.*, *110*, D20308, doi:10.1029/2005JD005875.

Wood, E. C., P. J. Wooldridge, J. H. Freese, T. Albrecht, and R. C. Cohen (2003), Prototype for in situ detection of atmospheric NO_3 and N_2O_5 via laser-induced fluorescence, *Environ. Sci. Technol.*, *37*(24), 5732–5738, doi:10.1021/es034507w.

Young, A. H., W. C. Keene, A. A. P. Pszenny, R. Sander, J. A. Thornton, T. P. Riedel, and J. R. Maben (2013), Phase partitioning of soluble trace gases with size-resolved aerosols in near-surface continental air over northern Colorado, USA, during winter, *J. Geophys. Res. Atmos.*, *118*, 9414–9427, doi:10.1002/jgrd.50655.

Young, C. J., et al. (2014), Chlorine as a primary radical: Evaluation of methods to understand its role in initiation of oxidative cycles, *Atmos. Chem. Phys.*, *14*(7), 3427–3440, doi:10.5194/acp-14-3427-2014.